Copy No. 176

RM No. A8F21

RM A8F21

CONFIDENTIAL

UNCLASSIFIED

UNCLASSIFIED

NACA RM No. A8F21

NACA

RESEARCH MEMORANDUM

AN EXPERIMENTAL INVESTIGATION AT LARGE SCALE OF SEVERAL CONFIGURATIONS OF AN NACA SUBMERGED AIR INTAKE

By Norman J. Martin and Curt A. Holzhauser

Ames Aeronautical Laboratory,
Moffett Field, Calif.

CANCELLED
Classification CHANGED TO Unclassified
By authority of Nasa Classification Ltr 9-21-54
Changed by Mo Date 8-22-55

CLASSIFIED DOCUMENT

This document contains classified information affecting the National Defense of the United States within the meaning of the Espionage Act, USC 50:31 and 32. Its transmission or the revelation of its contents in any manner to an unauthorized person is prohibited by law. Information so classified may be imparted only to persons in the military and naval services of the United States, appropriate civilian officers and employees of the Federal Government who have a legitimate interest therein, and to United States citizens of known loyalty and discretion who of necessity must be informed thereof.

UNCLASSIFIED

NATIONAL ADVISORY COMMITTEE FOR AERONAUTICS

WASHINGTON

October 19, 1948

CONFIDENTIAL

UNCLASSIFIED

NATIONAL ADVISORY COMMITTEE FOR AERONAUTICS

RESEARCH MEMORANDUM

AN EXPERIMENTAL INVESTIGATION AT LARGE SCALE OF SEVERAL CONFIGURATIONS OF AN NACA SUBMERGED AIR INTAKE

By Norman J. Martin and Curt A. Holzhauser

SUMMARY

An investigation of an NACA submerged air intake was conducted on a full-scale model of a fighter-type airplane. This study was made to determine the large-scale aerodynamic characteristics of a submerged air intake proposed as the result of small-scale tests and to compare the pressure-recovery characteristics of the large- and small-scale installations. Additional tests were made to determine the effect on pressure recovery of a systematic variation of ramp divergence.

The data obtained at various angles of attack and inlet-velocity ratios indicated the same favorable characteristics for the inlet that have been noted at small scale. The maximum values of entrance pressure recovery were high (92 percent for the full-scale inlet without deflectors), and the variation of pressure recovery with angle of attack and inlet-velocity ratio was small. Pressure recoveries measured with the full-scale model were approximately 5 percent higher than those measured with the small-scale model. It is shown that differences of boundary-layer thickness could account for 3 percent of this amount.

The tests in which the amount of ramp divergence was systematically varied indicated that varying the ramp divergence had only a small effect on the magnitude of the maximum pressure recovery measured at the entrance, but markedly changed the inlet-velocity ratio for maximum recovery. This change of inlet-velocity ratio resulted in higher maximum pressure recoveries after diffusion for the curved-divergent ramps than for the parallel-walled ramp.

An analysis of the data indicated that the use of deflectors on this model was not advantageous; the effect of an increased pressure recovery being outweighed by the external drag increment.

INTRODUCTION

The performance of a jet-powered or jet-assisted airplane depends

upon the efficiency attained in supplying air to the jet engine. Several types of inlets are capable of efficiently supplying air to a jet engine but have one or more of the following disadvantages:

1. A ducting system which severely handicaps the internal arrangement of the airplane

2. Large external drag increments

3. Insufficient area to handle the large quantities of air required for jet engines

In an effort to overcome these disadvantages with a minimum sacrifice of efficiency, submerged inlets were developed, and the results of experimental investigations of these inlets are presented in references 1 and 2. These references show the results of varying the many design parameters of NACA submerged inlets and the use of these results in design procedure. These results were obtained at small scale using a submerged entrance installed in one of the walls of a small wind-tunnel test section. A need for investigation of such inlets at large scale was apparent. Presented herein are the results of an investigation of the design parameters at large scale of an NACA submerged inlet installed on a model of a fighter-type airplane in the Ames 40- by 80-foot wind tunnel. The scope of the present investigation included the determination of the pressure-recovery characteristics of this submerged installation and the comparison of these characteristics with results obtained from small-scale tests of a similar air intake. In addition, tests were made to determine the effect on pressure recovery of a systematic variation of ramp divergence. Pressure-distribution measurements were also made from which critical Mach numbers of the various configurations were predicted.

SYMBOLS

α angle of attack referred to fuselage center line, degrees

a velocity of sound, feet per second

A duct area, square feet

d duct depth, inches

C_D drag coefficient $\left(\frac{D}{q_o S}\right)$

ΔC_D change in drag coefficient

H	total pressure $[p + q(1+\eta)]$, pounds per square foot
ΔH	loss in total pressure, pounds per square foot
D	drag of airplane, pounds
M	Mach number (V/a)
m	mass flow through duct (ρAV), slugs per second
p	static pressure, pounds per square foot
P	pressure coefficient $\left(\frac{p-p_o}{q_o}\right)$
ρ	mass density of air, slugs per cubic foot
q	dynamic pressure $\left(\frac{1}{2}\rho V^2\right)$, pound per square foot
S	wing area, square feet
V	velocity, feet per second
w	duct width, inches
y	distance above fuselage surface, inches
z	ramp width at beginning of ramp, inches
$(1+\eta)$	$\left(1 + \frac{M^2}{4} + \frac{M^4}{40} + \frac{M^6}{1600} - \frac{M^8}{80,000} \cdots\right)$
δ	boundary-layer thickness (distance from the fuselage where the velocity differs by 1 percent from the outer velocity at that station), inches
ζ	ramp divergence $\left[\left(1 - \frac{z}{w_1}\right) \times 100\right]$, percent

Subscripts

o	free stream
1	duct entrance (duct station 1)
2	assumed compressor inlet (duct station 2)
cr	critical

CONFIDENTIAL

Parameters

$\frac{H-p_o}{H_o-p_o}$ ram-recovery ratio

$\frac{V_1}{V_o}$ inlet-velocity ratio

η_D internal duct efficiency $\left(\frac{H_2-p_1}{H_1-p_1}\right)$ or $\left[1-\frac{\Delta H}{q_1(1+\eta_1)}\right]$

DESCRIPTION OF MODEL AND APPARATUS

The submerged entrance was located in one side of a full-scale model of a jet-propelled fighter airplane. The center of the submerged entrance was located 16 percent of the wing root chord forward and 21 percent of the wing root chord above the leading edge of the wing-fuselage juncture. A general view of the model mounted in the tunnel is shown in figure 1. A schematic drawing showing the general arrangements, instrumentation, and principal dimensions is presented in figure 2. Fuselage nose coordinates are presented in figure 3.

The geometrical characteristics of the submerged-entrance configurations are shown in figures 4, 5, 6, and 7. These characteristics can be defined by means of the following five parameters:

1. Width-to-depth ratio - the ratio of duct entrance width to entrance depth

2. Lip shape - the profile of the entrance lip

3. Distribution of ramp shape - the variation, with percent ramp length, of the nondimensional ordinates defining the ramp plan form

4. Ramp angle - the angle between the floor of the ramp and the extension of the fuselage contour line

5. Ramp divergence - a function of the ratio of the ramp width at the beginning of the ramp to the width of the duct entrance $[(1-\frac{z}{w_1})\times 100]$, percent

For all the configurations tested, the entrance area and the width–to–depth ratio were held constant at 0.667 square feet and 3.8, respectively. The lip shape, as shown in figure 6, was the same for all configurations. The distribution of ramp shape was fixed; that is, at any station, given in percent of the total length, the ratio of the ordinate to the maximum ordinate was constant. The shape distribution was related to the divergence in that the maximum ordinate was taken as the percent divergence, thus the ordinates for any divergence will be a constant percentage of the ordinates for 100–percent divergence.

For the series of plan forms shown in figure 4, the divergence was held constant at 91.7 percent, and the ramp length was varied such that ramp angles of 5°, 7°, and 9–1/2° were obtained. These plan forms, referred to herein as the standard curved–diverging ramp plan forms, have the same plan form as the curved–diverging ramp plan forms found to be satisfactory at small scale (reference 1). For the series of plan forms shown in figure 5, the ramp angle was held constant at 7°, and the divergence was varied from 0 percent (parallel walls) to a maximum of 98.7 percent.

Deflectors were constructed for the 7° and 9–1/2° ramps with standard divergence. The deflector coordinates are shown in figure 8. The design of the deflectors was based on shapes found to be satisfactory from tests on a small–scale model. (See reference 3.) Views showing the deflectors installed on the model are shown in figure 9.

The entrance station (duct station 1) was located 6–1/2 inches aft of the submerged–lip leading edge. The duct was of constant area from a station 3–1/2 inches forward to a station 3 inches aft of the entrance station. The pressure recovery was measured at the entrance station by 162 equally spaced total–pressure tubes and 25 static–pressure tubes. (See fig. 10.)

The rake used to measure pressure recovery at an assumed compressor inlet of the jet engine (duct station 2) contained 96 equally spaced total–pressure tubes and 40 static–pressure tubes. The ratio of duct area at this compressor station to area at the entrance was 1.52.

Total–pressure rakes were used to measure boundary–layer thickness on the basic fuselage. The basic fuselage contours were obtained by replacing the ramp and entrance by a filler block. The basic fuselage with the boundary–layer rakes installed is shown in figure 11.

Static pressure distributions along the ramp and over the lip contours were obtained by means of flush orifices located along the center line of the ramp and center line of the lip inner and outer surfaces. (See fig. 6 for lip orifice stations.) Additional static pressure distributions over the lip inner and outer surfaces were obtained with similar flush orifices located 25 percent of the duct width (4-3/4 in.) from the center line of the duct.

Total-pressure tubes, used in obtaining ram recovery, were connected to an integrating water-in-glass manometer which provided an arithmetic mean value of loss of total pressure. Individual tube readings of this integrating manometer and all other manometers were recorded photographically.

The internal-flow system included an axial-flow fan which was necessary to provide the desired range of inlet-velocity ratios. Flow control was obtained by varying the speed and direction of rotation of the motors. The quantity of internal air flow was computed from the readings of 20 equally spaced total-pressure tubes and 8 static-pressure tubes at the air outlet.

TESTS

In order to evaluate the effect of entrance conditions on the duct losses, the internal duct efficiency was determined prior to installation of the duct in the model. An entrance nozzle was attached to the duct entrance in place of the ramp and lip to assure satisfactory flow conditions at the entrance. The pressure losses were measured at an assumed compressor inlet (duct station 2), using the rake employed to measure pressure recovery at that station during the tunnel tests.

The aerodynamic characteristics of the standard curved-diverging ramp configurations, with and without deflectors, and of the 7° ramp with no divergence were determined for a large number of flight conditions. Data which included pressure-recovery characteristics at the entrance and at the assumed compressor inlet, and pressure distribution over the ramp and lip surfaces were obtained for an inlet-velocity-ratio range of 0.2 to 1.6 and an angle-of-attack range of -2° to 9°. These data were obtained at free-stream velocities of approximately 110, 160, and 225 miles per hour to illustrate the effects of Reynolds number. The entrance rake was removed from the duct during measurements of pressure recovery at duct station 2. Drag measurements were made to determine the incremental drag resulting from the installation of deflectors.

The effect of varying the divergence of the 7° ramp was determined by making pressure-recovery measurements at the entrance station throughout an inlet-velocity-ratio range of 0.2 to 1.6 with the airplane at constant angle of attack (-2°) and with a constant air-stream velocity of 160 miles per hour.

The effect of a thickened boundary layer on the pressure-recovery characteristics measured at duct station 2 was investigated by thickening the boundary layer by means of a quarter-inch cotton rope wrapped around the fuselage at station 27. The boundary-layer thickness was determined on the basic fuselage at station 158.25. Boundary-layer measurements were made for both the normal and the thickened boundary-layer conditions.

RESULTS AND DISCUSSION

Reduction of Data

Throughout this report the pressure-recovery values considered are those obtained from the arithmetic average of the total pressures indicated by the various tubes. As shown in reference 1, such values are not exact since the true pressure recovery is also a function of the mass flow at each point. For the subject tests the pressure-recovery values obtained by using the arithmetic average readings were lower than the values obtained by weighted integration of the total pressures, the average deviation for a series of conditions chosen at random being of the order of 2 percent with the maximum deviation being 5 percent. Since the arithmetic average values of pressure recovery were conservative and their use in making comparisons and showing trends introduced only minor errors, it was felt that the additional work required for the more exact reduction of the data was not justified.

Measurements of entrance ram-recovery ratio at inlet-velocity ratios below 0.4 were characterized by wide fluctuations; therefore, values obtained at these low inlet-velocity ratios are not usable. It is not known to what extent these fluctuations may have been caused by the entrance characteristics or by the internal duct characteristics. Similar fluctuations were not observed during the small-scale tests (references 1 and 2) indicating that the disturbance was caused by a poor characteristic of the ducting system, such as the sudden expansion of the air as it entered the blower or pulsation of flow resulting from inadequate control of the flow velocity at low inlet-velocity ratios. Since pressure recovery after diffusion did not show these fluctuations at low inlet-velocity

ratios, the data obtained at assumed compressor inlet (duct station 2) together with the internal duct efficiency were used to determine the entrance pressure-recovery variation in the low-inlet-velocity-ratio range.

Pressure-Recovery Characteristics

Effect of inlet-velocity ratio on pressure recovery at constant angle of attack.- The variation of entrance ram-recovery ratios with inlet-velocity ratio is shown in figures 12(a) and (b) for all ramp configurations tested. For clarity of presentation, the test points were omitted from figure 12(b) and the exact values are given in table I. All data presented were obtained at a free-stream velocity of approximately 160 miles per hour and at the angle of attack, -2°, for zero lift. The data at other free-stream velocities are not presented because of the close agreement with the data presented.

It may be noted from figures 12(a) and (b) that changes of ramp angle and ramp divergence had only a minor effect on the magnitude of the maximum ram recovery at the entrance station The main effect of increasing the ramp divergence with a fixed ramp angle (fig. 12(b)) was to decrease the pressure recovery at inlet-velocity ratios above 0.95 and to increase the pressure recovery at inlet-velocity ratios below 0.75, resulting in a change of inlet-velocity ratio at which the ram recovery was a maximum. For example, the inlet-velocity ratio for maximum ram-recovery ratio was 0.50 for the 7° ramp with 98.7-percent divergence compared to 1.60 for the 7° ramp with no divergence. Increasing ramp angle similarly changed the inlet-velocity ratio for maximum ram recovery, but to a considerably lesser extent. As will be discussed later, this change of inlet-velocity ratio for maximum ram recovery at the entrance station is of importance with regard to the maximum ram recovery at the assumed compressor inlet (duct station 2).

Aside from the effect of the ramp configuration on the maximum ram-recovery characteristics at the entrance, there is also an effect of the ramp configuration on the variation of ram recovery with inlet-velocity ratio. Increasing the divergence reduced the variation of ram-recovery ratio with inlet-velocity ratio over a representative portion of the inlet-velocity-ratio range (0.4 to 1.6). The variation of ram-recovery ratio was reduced from 0.16 for the 7° ramp with no divergence to 0.04 for the 7° ramp with 80-percent divergence. Further increase of divergence did not result in any

appreciable change in the variation.

The variation of ram-recovery ratio measured at the assumed compressor station (duct station 2) with inlet-velocity ratio is presented in figure 13 for the 5°, 7°, and 9-1/2° ramps with standard divergence and for the 7° ramp with no divergence. A comparison of figures 12 and 13 illustrates that the effect of the diffuser on pressure recovery of the divergent-type entrances was to reduce the maximum ram-recovery ratio by 0.02 and to change the inlet-velocity ratio for maximum recovery by only a negligible amount. However, with the parallel-sided entrance, the diffuser reduced the maximum ram-recovery ratio by 0.09 and changed the inlet-velocity ratio for maximum recovery from 1.6 to 0.8. Thus, with the maximum ram-recovery ratio of the same magnitude at the entrance station for the two different ramp plan forms having the same ramp angle (7°), the divergent-type entrance had the advantage of a higher maximum ram-recovery ratio after diffusion.

This advantage of higher over-all system efficiency is attributable to the lower inlet-velocity ratio at which the entrance ram-recovery ratio for the divergent-type inlet is a maximum and the consequent lower internal duct losses. As shown in figure 14, the internal duct losses were a constant percentage of the entrance dynamic pressure. In addition, as shown in figure 15, the entrance conditions had only a minor effect on the internal duct efficiency. As a result, the duct losses in terms of free-stream dynamic pressure vary directly as the square of the inlet-velocity ratio. The internal duct losses at maximum recovery were, therefore, greater for the parallel-sided inlet than for the divergent-type inlet. This point is illustrated in figure 16. With a duct having an internal duct efficiency of 91 percent, such as was used on the test installation, the system using the paralled-sided inlet at the inlet-velocity ratio for maximum entrance ram recovery (1.6) incurs the high internal duct losses associated with high inlet-velocity ratios. However, the use of the divergent-type inlet with high pressure recovery at low inlet-velocity ratios, where internal duct losses are much smaller, enables the over-all system efficiency to be higher at an inlet-velocity ratio of 0.9 or less. With less efficient ducts, such as are likely to be used, the advantage of the divergent-type inlets would be greater.

It should be noted that the comparisons of the maximum recovery values were made without regard to the fact that they occurred at different quantities of flow. From a design standpoint, however, comparisons should be made with the same rate of flow at the compressor. The results of duct tests (reference 4) indicate that

the efficiency of the duct used for the subject tests approaches the maximum that can be expected for a diffusing duct with high rates of flow. An increase of the diffusion in the ducting system of the parallel-sided inlet would be required to make the parallel-sided inlet operate at an inlet-velocity ratio for maximum entrance ram recovery and at the same time have a flow rate at the compressor equal to that of the divergent-type inlet operating at an inlet-velocity ratio for maximum entrance ram recovery. It follows that this new duct would incur greater losses and would make the system using a parallel-sided inlet have even greater losses than presently shown.

Effect of angle of attack on pressure recovery.- The variation of ram recovery with angle of attack is presented in figure 17 and tables II and III. There was a small variation of ram-recovery ratio with angle of attack throughout the investigated inlet-velocity-ratio range. Two representative values of lift coefficient were $C_L = 0$ at -2° angle of attack and $C_L = 0.93$ at 9° angle of attack.

Effect of deflectors.- It is shown in figure 18 that the effect of adding deflectors to the divergent-type intakes was to increase the maximum ram-recovery ratio at the entrance by 0.04 (from 0.92 to 0.96 for the 7° ramp and 0.91 to 0.95 for the $9\text{-}1/2^\circ$ ramp) and to increase the inlet-velocity ratio at which maximum recovery was obtained. The increased duct losses associated with the higher inlet-velocity ratio resulted in the deflectors effecting only a 0.01 increase of maximum ram-recovery ratio (from 0.91 to 0.92 for the divergent ramps) at duct station 2. The addition of deflectors also resulted in an increase in ram-recovery ratio for inlet-velocity ratios from approximately 0.55 to 1.40, the maximum increase for both ramps being 0.08 and occurring at an inlet-velocity ratio of 0.90 for the 7° ramp and 0.75 for the $9\text{-}1/2^\circ$ ramp.

In contemplating the use of deflectors, the increase in ram recovery and consequent increase in thrust output must be weighed against the increased external drag that may be caused by deflectors. The deflectors, shown in figure 9, form a protrusion on the fuselage and cause additional external drag as shown in figure 19. (By use of the blower, the internal drag, as defined in reference 5, was held constant at a given inlet-velocity ratio for each configuration.)

The calculated effect of these deflectors on the propulsive thrust of an airplane using two similarly located submerged inlets to supply air to a turbojet engine is shown in the following table:

Airplane speed at sea level (mph)	350	400	450	500	550	600
Inlet-velocity ratio	1.165	1.020	0.900	0.800	0.735	0.670
$\frac{\text{Increase in drag}}{\text{Jet thrust available}}$	.020	.036	.061	.096	.132	.167
$\frac{\text{Increase in jet thrust}}{\text{Jet thrust available}}$	.013	.029	.040	.042	.039	.035
$\frac{\text{Thrust gain-drag increase}}{\text{Jet thrust available}}$	-.007	-.007	-.021	-.054	-.093	-.132

The method of calculating the effect of deflectors on the net thrust is presented in Appendix A and reference 6. As shown in the preceding table, the use of deflectors on this type of installation would result in a decrease of propulsive thrust at all probable velocities of an airplane using the present submerged inlets.

Effect of increased boundary-layer thickness.- The distribution of ram recovery in the normal boundary layer and the thickened boundary layer is shown in figure 20. The reduction of ram-recovery ratio at the assumed compressor inlet caused by the thickening of the boundary layer is shown in figure 21. It would be expected that approximately the same reduction of ram recovery would be measured at the entrance station, for, as shown previously, changes in pressure recovery at the entrance had very little effect on the internal duct efficiency.

Calculations indicate that the use of the empirical equation

$$\Delta\left(\frac{H_2-p_o}{H_o-p_o}\right) = \left(\frac{H_2-p_o}{H_o-p_o}\right)_a - \left(\frac{H_2-p_o}{H_o-p_o}\right)_b = \left(\frac{h}{d}\right)_a - \left(\frac{h}{d}\right)_b$$ [1]

[1] a and b represent two different boundary-layer conditions, and h is defined as a height of an area of unit width in which the complete loss of free-stream ram pressure is equivalent to the integrated loss of total pressure in unit width of the boundary layer, or

$$h = \int_o^{\delta} \frac{H_o-H}{H_o-p_o}\,dy$$

will give a first approximation of the change in pressure recovery due to thickening of the boundary layer. The values of $\frac{h}{d}$ for the normal and thickened boundary layers are 0.078 and 0.104, respectively. A comparison of the calculated and measured changes in ram-recovery ratio caused by thickening the boundary layer is given in the following table for the 7° ramp with standard divergence:

V_1/V_0	$\Delta\left(\frac{H_2-p_0}{H_0-p_0}\right)$	
	Calculated	Measured
0.6	0.026	0.030
.8	.026	.027
1.0	.026	.026

It is felt that the change in boundary-layer thickness produced would be the maximum that would result from manufacturing irregularities; therefore, for entrance locations and body shapes similar to the present model, the effect of manufacturing irregularities on pressure recovery is of secondary importance.

Comparison with small-scale results.- The similarity of the pressure-recovery characteristics measured at the submerged entrance of the full-scale model with those measured on the small-scale model (reference 1) can be seen in figure 22. Although the values of ram-recovery ratio obtained with the full-scale model are approximately 5 percent higher than those obtained with the small-scale model, the variation of pressure recovery with inlet-velocity ratio and with configuration changes are very similar. Part of the increased pressure recovery measured with the full-scale model is due to the smaller boundary-layer thickness relative to the duct depth. (The values of $\frac{h}{d}$ for the full-scale model and small-scale model were 0.078 and 0.112, respectively, accounting for 3.4 percent of the increase in pressure recovery.) The remaining portion can probably be accounted for by differences of loss distribution in the boundary layers of the two models. (See fig. 20.)

Pressure Distribution and Critical Mach Number

Estimations of the critical Mach number characteristics of the various parts of the submerged entrances were made from the peak

negative pressure coefficients using the Kármán–Tsien method. (See reference 7.) Although this method is not entirely applicable to three–dimensional flow, it is believed that estimations of critical Mach number using this method are conservative. Furthermore, it is shown in reference 5 that with a submerged inlet installation on a model of a fighter airplane, Mach numbers as much as 0.055 higher than the maximum estimated critical Mach number of this report were reached without seriously affecting the pressure recovery or the drag.

Lip.– Pressure distribution over the lip inner and outer surfaces are presented in figure 23 and tables IV, V, VI, and VII. The variation of predicted critical Mach number with inlet–velocity ratio at the center line of the lip (fig. 24) indicates that the predicted critical Mach number characteristics are very similar to those obtained on the small–scale models even though minor differences of lip contour existed. As was noted previously (reference 1), the ramp angle has a large effect on the angle of flow approaching the lip. For the lip tested, increasing the ramp angle increased the maximum critical Mach number of the lip. It is possible that varying the lip incidence would have increased the maximum critical Mach number with the lower ramp angles without adversely affecting the pressure recovery.

Static pressure distribution measured over the inner and outer surface at a distance of 25 percent of the duct width on either side of the lip center line indicated critical Mach numbers very similar to those obtained at the lip center line and are, therefore, not presented.

Ramp.– Pressure distribution along the center line of the ramps is presented in figure 25 for one inlet–velocity ratio, 0.74. As may be noted, the peak negative pressure coefficient occurs at the beginning of the ramp. The measurements at other inlet–velocity ratios showed that this pressure was independent of inlet–velocity ratio. With a constant curvature at the beginning of the ramp, the magnitude of this peak pressure is influenced by both the ramp angle and the basic fuselage pressure field. Increasing the ramp angle increases the difference between the peak pressure and the basic fuselage static pressure at the beginning of the ramp. However, if the smaller ramp angle with its attendant longer ramp results in the beginning of the ramp being located in a region of higher velocities, as was the case with the 5° ramp, any gain in critical Mach number reasonably expected by using a smaller ramp angle may be nullified. This effect on the critical Mach number is shown in the following table:

Configuration	M_{cr}
5° ramp, standard divergence	0.77
7° ramp, standard divergence	.82
9-1/2° ramp, standard divergence	.78
7° ramp, no divergence	.82

CONCLUDING REMARKS

An experimental investigation at large scale of certain configuration changes and parameters affecting the characteristics of NACA submerged inlets indicates that the data obtained at large scale are similar to the data obtained at small scale in the following respects:

1. There was good recovery of the free-stream ram pressure (the maximum pressure recovery at the entrance being 92 percent for the full-scale inlet without deflectors).

2. The variation of the entrance pressure recovery with both inlet-velocity ratio and angle of attack was small.

3. The maximum value of entrance pressure recovery was essentially unaffected by changes of ramp-wall divergence.

4. Increasing the ramp-wall divergence decreased the inlet-velocity ratio for maximum entrance pressure recovery, resulting in a higher maximum recovery after diffusion for the standard curved-divergent ramp than for the parallel-walled ramp.

These similarities indicate that the data obtained at small scale are satisfactory for design purposes.

The large-scale and small-scale results disagreed in the actual magnitude of the pressure recoveries; the large-scale values were generally about 5 percent higher. Of this amount, 3 percent was accounted for by a simple approximation which considered the effects on pressure recovery of the difference in boundary-layer thickness between the two models.

It was noted that deflectors were also effective at large scale in increasing the pressure recovery. Calculations indicated that

the associated external drag increase due to the deflectors outweighed the favorable effect of the increased pressure recovery.

Ames Aeronautical Laboratory,
National Advisory Committee for Aeronautics,
Moffett Field, Calif.

APPENDIX A

Calculation of the Effect of Deflectors on the Net Thrust of Airplane

Calculations were based on the assumption that an airplane of 275 square feet wing area was flying at sea level and twin submerged air intakes with 7° standard curved-divergent ramps were supplying air to a turbojet engine. The turbojet engine used in these calculations had a military rated thrust of 3000 pounds at sea-level static condition which required an air flow of 52 pounds per second. The effect of changes of pressure recovery on the net thrust was calculated from data presented in reference 6.

It was determined that changes of angle of attack to produce lift coefficients necessary to maintain flight had negligible effects on the increment of drag caused by the deflectors. Therefore, for this analysis it was assumed that the drag increment varied with inlet-velocity ratio as shown in figure 19 for the various assumed flight speeds.

REFERENCES

1. Mossman, Emmet A., and Randall, Lauros M.: An Experimental Investigation of the Design Variables for NACA Submerged Duct Entrances. NACA RM No. A7I30, 1948.

2. Frick, Charles W., Davis, Wallace F., Randall, Lauros M., and Mossman, Emmet A.: An Experimental Investigation of NACA Submerged-Duct Entrances. NACA ACR No. 5I20, 1945.

3. Delaney, Noel K.: An Investigation of Submerged Air Inlets on a 1/4-Scale Model of a Typical Fighter-Type Airplane. NACA RM No. A8A20, 1948.

4. Patterson, G. N.: Modern Diffuser Design. Aircraft Engineering. vol. 10, no. 115, Sept. 1938, pp. 267-273.

5. Hall, Charles F., and Barclay, F. Dorn: An Experimental Investigation of NACA Submerged Inlets at High Subsonic Speeds. I - Inlets Forward of the Wing Leading Edge. NACA RM No. A8B16, 1948.

6. Hanson, Frederick H., Jr., and Mossman, Emmet A.: Effect of Pressure Recovery on the Performance of a Jet-Propelled Airplane. NACA TN No. 1695, 1948.

7. von Kármán, Th.: Compressibility Effects in Aerodynamics. Jour. Aero. Sci., vol. 8, no. 9, July 1941, pp. 337-356.

TABLE I.- THE VARIATION OF ENTRANCE RAM-RECOVERY RATIO WITH INLET-VELOCITY RATIO FOR SEVERAL AMOUNTS OF DIVERGENCE OF THE 7° RAMP

$\alpha = -2^\circ$						
V_1/V_o	Ramp Divergence					
	20%	40%	60%	80%	96%	98.7%
0.12	- - -	0.557	0.598	0.712	0.777	- - -
.21	0.570	.630	.685	.787	.841	0.845
.40	.732	.782	.820	.871	.899	.897
.50	.798	.840	.868	.894	.927	.933
.55	- - -	- - -	- - -	- - -	.929	.930
.61	.851	.882	.901	.914	.926	.925
.70	.869	.892	.901	.906	.910	.911
.81	.882	.891	.896	.891	.894	- - -
1.01	.890	.889	.890	.885	.881	.878
1.21	.896	.894	.895	.889	.883	.878
1.41	.905	.901	.901	.894	.882	.882
1.56	.908	.904	.904	.894	- - -	.882

TABLE II.- THE VARIATION OF ENTRANCE RAM-RECOVERY RATIO WITH INLET-VELOCITY RATIO FOR SEVERAL ANGLES OF ATTACK

5° Ramp, Standard Divergence						
V_1/V_0 \ α	−4°	−2°	0°	2°	5°	9°
0.61	0.913	0.923	0.913	0.889	0.838	0.774
.67	.920	.924	.911	.885	.839	.801
.74	.918	.917	.904	.879	.827	.799
.87	.906	.903	.892	.872	.822	.776
1.00	.898	.899	.883	.873	.821	.754
1.20	.896	.894	.884	.866	.821	.740
1.40	.896	.893	.880	.866	.822	.732
1.60	.896	.895	.883	.860	.820	.730
7° Ramp, Standard Divergence						
V_1/V_0 \ α	−4°	−2°	0°	2°	5°	9°
0.61	0.916	0.922	0.929	0.880	0.843	0.804
.67	.911	.917	.900	.873	.834	.798
.74	.897	.902	.887	.863	.812	.782
.87	.888	.881	.872	.855	.809	.755
1.00	.880	.874	.867	.843	.801	.717
1.20	.877	.874	.863	.842	.791	— — —
1.40	.871	.872	.856	.836	.781	— — —
1.60	.871	.872	.856	.836	.777	— — —

TABLE II.- Concluded.

$9\frac{1}{2}^\circ$ Ramp, Standard Divergence						
V_1/V_o \ α	-4°	-2°	0°	2°	5°	9°
0.61	0.869	0.882	0.861	0.821	0.738	0.723
.67	.859	.865	.850	.816	.736	.731
.74	.851	.852	.838	.810	.738	.669
.87	.854	.850	.837	.815	.770	.677
1.00	.846	.840	.828	.804	.753	- - -
1.20	.842	.836	.820	.797	.744	- - -
1.40	.831	.832	.812	.781	.722	- - -
1.60	- - -	.831	- - -	- - -	- - -	- - -
7° Ramp, No Divergence						
V_1/V_o \ α	-4°	-2°	0°	2°	5°	9°
0.61	0.800	0.824	0.784	0.751	- - -	- - -
.67	.840	.837	.821	.796	- - -	- - -
.74	.854	.861	.839	.814	- - -	- - -
.87	.877	.883	.867	.841	- - -	- - -
1.00	.892	.892	.880	.859	- - -	- - -
1.20	.904	.902	.886	.869	- - -	- - -
1.40	.914	.909	.897	.877	- - -	- - -
1.60	.917	.916	.900	.880	- - -	- - -

TABLE III.- THE VARIATION OF RAM-RECOVERY RATIO MEASURED AFTER DIFFUSION WITH INLET-VELOCITY RATIO FOR SEVERAL ANGLES OF ATTACK

5° Ramp, Standard Divergence						
α / V_1/V_o	-4°	-2°	0°	2°	5°	9°
0.52	0.887	0.883	- - -	0.867	- - -	0.799
.61	.889	.898	0.887	.867	- - -	.783
.67	- - -	.886	- - -	- - -	- - -	- - -
.74	.860	.869	.857	.831	- - -	.747
.87	.827	.831	.821	.798	- - -	.688
1.00	.800	.801	.797	.781	- - -	.640
1.20	.766	.767	.760	.743	- - -	.598
1.40	.717	.724	.713	.701	- - -	.555
1.60	.670	.676	.662	.649	- - -	.509
7° Ramp, Standard Divergence						
α / V_1/V_o	-4°	-2°	0°	2°	5°	9°
0.52	0.890	0.899	0.890	0.862	0.833	0.796
.61	.888	.897	.883	.860	.825	.792
.67	- - -	.875	.865	- - -	- - -	- - -
.74	.846	.854	.841	.816	.774	.747
.87	.808	.807	.796	.779	.727	.660
1.00	.778	.779	.769	.751	.696	.583
1.20	.747	.748	.733	.714	.652	.537
1.40	.697	.703	.692	.679	.609	.486
1.60	.659	.659	.638	.618	.557	.455

TABLE III.- Concluded.

$9\frac{1}{2}^\circ$ Ramp, Standard Divergence						
V_1/V_0 \ α	-4°	-2°	0°	2°	5°	9°
0.52	0.873	0.893	0.870	0.829	0.747	0.762
.61	.843	.854	.838	.806	.733	.736
.67	- - -	- - -	- - -	- - -	- - -	- - -
.74	.792	.800	.786	.770	.699	.657
.87	.766	.764	.752	.729	.676	.593
1.00	.732	.735	.721	.697	.636	.516
1.20	.702	.702	.686	.658	.584	.459
1.40	.650	.651	.640	.612	.534	.372
1.60	.605	.607	.592	.564	.494	- - -
7° Ramp, No Divergence						
V_1/V_0 \ α	-4°	-2°	0°	2°	5°	9°
0.52	- - -	- - -	- - -	- - -	- - -	- - -
.61	0.780	0.784	0.754	0.739	0.714	- - -
.67	.799	.802	.773	.760	.726	- - -
.74	.810	.810	.795	.765	.734	- - -
.87	.810	.811	.795	.776	.738	- - -
1.00	.790	.799	.787	.776	.726	- - -
1.20	.769	.768	.759	.749	.709	- - -
1.40	.754	.734	.725	.714	.676	- - -
1.60	.686	.685	.669	.666	.625	- - -

TABLE IV.- THE VARIATION OF PRESSURE COEFFICIENT ALONG THE CENTER LINE OF THE LIP WITH ANGLE OF ATTACK AND INLET-VELOCITY RATIO FOR THE 5° RAMP WITH STANDARD DIVERGENCE

$\alpha = -2°$								
Distance aft of lip leading edge (in.)	Inlet-Velocity Ratio, V_1/V_o							
	0.54	0.61	0.67	0.74	0.87	1.00	1.20	1.40
[1]0.00	0.67	0.82	--	0.98	1.00	0.90	0.61	0.05
[1] .10	-.20	.03	--	.40	.71	.88	.98	1.00
[1] .25	-.61	-.39	--	-.02	.32	.54	.76	.93
[1] .50	-.75	-.57	--	-.29	-.01	.19	.41	.62
[1]1.00	-.67	-.55	--	-.36	-.17	-.02	.14	.31
[1]1.50	-.54	-.45	--	-.31	-.17	-.07	.06	.19
[1]2.50	-.30	-.29	--	-.20	-.11	-.04	.04	.12
[1]5.00	-.14	-.11	--	-.06	-.02	.01	.04	.09
[1]7.50	-.07	-.05	--	-.02	.01	.02	.05	.08
[2] .10	.98	.93	--	.72	.34	-.12	-.89	-1.99
[2] .25	.84	.75	--	.45	-.02	-.54	-1.36	-2.50
[2] .50	.68	.59	--	.27	-.19	-.68	-1.42	-2.42
[2]1.00	.55	.45	--	.15	-.28	-.72	-1.37	-2.24
[2]1.50	.48	.40	--	.10	-.31	-.73	-1.34	-2.17
[2]2.50	.46	.39	--	.11	-.26	-.65	-1.21	-1.88
[2]5.00	.52	.45	--	.23	-.07	-.39	-.88	-1.50
[2]7.50	.64	.58	--	.39	.13	-.13	-.52	-1.03

[1] Outside Contour

[2] Inside Contour

TABLE IV.- Continued.

$\alpha = 0^\circ$								
Distance aft of lip leading edge (in.)	Inlet-Velocity Ratio, V_1/V_o							
	0.54	0.61	0.67	0.74	0.87	1.00	1.20	1.40
[1]0.00	--	0.78	--	0.97	1.00	1.00	0.67	0.12
[1] .10	--	-.05	--	.35	.68	.84	.99	1.00
[1] .25	--	-.49	--	-.09	.26	.47	.82	.91
[1] .50	--	-.68	--	-.37	-.10	.11	.36	.57
[1]1.00	--	-.65	--	-.45	-.27	-.11	.08	.25
[1]1.50	--	-.55	--	-.40	-.27	-.15	--	.13
[1]2.50	--	-.36	--	-.27	-.19	-.12	-.02	.07
[1]5.00	--	-.18	--	-.12	-.10	-.07	-.02	.02
[1]7.50	--	-.13	--	-.10	-.08	-.05	-.01	--
[2] .10	--	.93	--	.57	.37	-.08	-.85	-1.94
[2] .25	--	.75	--	.40	-.01	-.49	-1.31	-2.46
[2] .50	--	.59	--	.27	-.19	-.64	-1.40	-2.40
[2]1.00	--	.49	--	.14	-.28	-.69	-1.36	-2.25
[2]1.50	--	.43	--	.09	-.33	-.71	-1.34	-2.17
[2]2.50	--	.42	--	.10	-.28	-.63	-1.21	-1.95
[2]5.00	--	.46	--	.22	-.08	-.38	-.87	-1.51
[2]7.50	--	.58	--	.39	.13	-.12	-.51	-1.03

[1] Outside Contour

[2] Inside Contour

TABLE IV.- Concluded.

$\alpha = 2^{\circ}$								
Distance aft of lip leading edge (in.)	Inlet-Velocity Ratio, V_i/V_o							
	0.54	0.61	0.67	0.74	0.87	1.00	1.20	1.40
[1]0.00	0.71	0.79	--	0.97	1.00	0.94	0.68	0.16
[1] .10	-.19	-.06	--	.33	.62	.80	.97	1.00
[1] .25	-.65	-.51	--	-.14	.18	.41	.68	.87
[1] .50	-.84	-.73	--	-.44	-.18	.03	.29	.51
[1]1.00	-.80	-.72	--	-.52	-.34	-.20	--	.18
[1]1.50	-.68	-.61	--	-.48	-.34	-.24	-.09	.06
[1]2.50	-.47	-.44	--	-.36	-.27	-.20	-.11	-.01
[1]5.00	-.27	-.25	--	-.22	-.18	-.16	-.11	-.05
[1]7.50	-.22	-.21	--	-.18	-.16	-.14	-.12	-.08
[2] .10	.97	.93	--	.72	.38	-.03	-.83	-2.88
[2] .25	.80	.74	--	.43	.01	-.45	-1.24	-2.41
[2] .50	.64	.60	--	.25	-.18	-.60	-1.40	-2.28
[2]1.00	.50	.43	--	.12	-.28	-.65	-1.38	-2.21
[2]1.50	.44	.37	--	.08	-.31	-.66	-1.33	-2.13
[2]2.50	.43	.37	--	.10	-.25	-.59	-1.21	-1.93
[2]5.00	.50	.46	--	.22	-.06	-.34	-.86	-1.47
[2]7.50	.62	.57	--	.37	.13	-.09	-.51	-1.00

[1]Outside Contour
[2]Inside Contour

TABLE V.- THE VARIATION OF PRESSURE COEFFICIENT ALONG THE CENTER LINE OF THE LIP WITH ANGLE OF ATTACK AND INLET-VELOCITY RATIO FOR THE 7° RAMP WITH STANDARD DIVERGENCE

$\alpha = -2°$								
Distance aft of lip leading edge (in.)	Inlet-Velocity Ratio, V_1/V_o							
	0.54	0.61	0.67	0.74	0.87	1.00	1.20	1.40
[1]0.00	--	0.94	0.99	0.92	0.95	0.80	0.34	-.29
[1] .10	--	.34	.49	.61	.84	.95	1.00	.95
[1] .25	--	-.05	.10	.23	.47	.69	.89	.98
[1] .50	--	-.30	-.19	-.08	.14	.34	.57	.73
[1]1.00	--	-.37	-.29	-.21	-.06	.09	.28	.34
[1]1.50	--	-.31	-.26	-.21	-.08	.02	.16	.29
[1]2.50	--	-.21	-.16	-.13	-.06	.02	.11	.20
[1]5.00	--	-.05	-.04	-.05	-.01	.03	.12	.12
[1]7.50	--	-.02	-.01	--	.01	.03	.07	.98
[2] .10	--	.82	.73	.56	.16	-.34	-1.32	-2.42
[2] .25	--	.60	.44	.27	-.19	-.81	-1.74	-2.85
[2] .50	--	.45	.30	.11	-.30	-.80	-1.69	-2.65
[2]1.00	--	.35	.21	.04	-.34	-.77	-1.55	-2.26
[2]1.50	--	.32	.19	.03	-.34	-.75	-1.47	-2.14
[2]2.50	--	.67	.22	.04	-.25	-.63	-1.20	-1.85
[2]5.00	--	.47	.37	.25	-.03	-.34	-.87	-1.43
[2]7.50	--	.55	.45	.34	.10	-.16	-.63	-1.13

[1]Outside Contour
[2]Inside Contour

TABLE V.- Continued.

$\alpha = 0^\circ$								
Distance aft of lip leading edge (in.)	Inlet-Velocity Ratio, V_1/V_o							
	0.54	0.61	0.67	0.74	0.87	1.00	1.20	1.40
[1]0.00	--	0.93	0.99	1.00	0.98	0.83	0.44	-.19
[1] .10	--	.26	.44	.59	.82	.99	1.00	.99
[1] .25	--	-.17	.02	.18	.45	.64	.85	.98
[1] .50	--	-.43	-.28	-.14	.09	.28	.50	.69
[1]1.00	--	-.48	-.38	-.28	-.12	.02	.20	.38
[1]1.50	--	-.43	-.35	-.28	-.15	-.04	.09	.23
[1]2.50	--	-.30	-.25	-.20	-.12	-.04	.05	.14
[1]5.00	--	-.14	-.13	-.12	-.07	-.03	.02	.07
[1]7.50	--	-.11	-.08	-.08	-.06	-.03	-.01	.25
[2] .10	--	.84	.72	.56	.16	-.32	-1.19	-2.31
[2] .25	--	.63	.46	.26	-.21	-.73	-1.63	-2.77
[2] .50	--	.47	.30	.10	-.33	-.80	-1.60	-2.58
[2]1.00	--	.37	.21	.03	-.37	-.79	-1.48	-2.27
[2]1.50	--	.33	.18	.01	-.37	-.75	-1.41	-2.12
[2]2.50	--	.36	.22	.06	-.28	-.63	-1.14	-1.82
[2]5.00	--	.48	.37	.23	-.04	-.34	-.83	-1.40
[2]7.50	--	.56	.45	.33	.09	-.17	-.59	-1.10

[1] Outside Contour
[2] Inside Contour

TABLE V.- Concluded.

$\alpha = 2^{\circ}$								
Distance aft of lip leading edge (in.)	Inlet-Velocity Ratio, V_1/V_0							
	0.54	0.61	0.67	0.74	0.87	1.00	1.20	1.40
[1]0.00	--	0.93	0.98	1.00	0.97	0.83	0.45	-.17
[1] .10	--	.26	.42	.58	.77	.92	.99	.98
[1] .25	--	-.18	-.03	.14	.38	.60	.82	.94
[1] .50	--	-.46	-.33	-.20	.02	.22	.45	.64
[1]1.00	--	-.55	-.45	-.35	-.20	-.04	.13	.31
[1]1.50	--	-.49	-.43	-.35	-.24	-.12	.02	.15
[1]2.50	--	-.37	-.32	-.27	-.20	-.12	-.03	.07
[1]5.00	--	-.23	-.22	-.20	-.16	-.11	-.08	-.02
[1]7.50	--	-.19	-.18	-.17	-.15	-.12	-.10	-.06
[2] .10	--	.80	.69	.53	.19	-.31	-1.20	-2.29
[2] .25	--	.58	.43	.23	-.17	-.71	-1.65	-2.77
[2] .50	--	.42	.27	.07	-.30	-.79	-1.62	-2.58
[2]1.00	--	.32	.18	.00	-.34	-.77	-1.48	-2.27
[2]1.50	--	.30	.15	-.02	-.33	-.74	-1.42	-2.11
[2]2.50	--	.33	.20	.04	-.24	-.61	-1.14	-1.80
[2]5.00	--	.46	.35	.23	-.01	-.31	-.87	-1.39
[2]7.50	--	.53	.43	.32	.12	-.15	-.59	-1.10

[1]Outside Contour
[2]Inside Contour

TABLE VI.- THE VARIATION OF PRESSURE COEFFICIENT ALONG THE CENTER LINE OF THE LIP WITH ANGLE OF ATTACK AND INLET-VELOCITY RATIO FOR THE $9\frac{1}{2}^{\circ}$ RAMP WITH STANDARD DIVERGENCE

$\alpha = -2^{\circ}$								
Distance aft of lip leading edge (in.)	Inlet-Velocity Ratio, V_1/V_o							
	0.54	0.61	0.67	0.74	0.87	1.00	1.20	1.40
[1]0.00	0.98	1.00	1.00	0.98	0.84	0.57	-.03	-.92
[1] .10	.50	.62	.73	.81	.94	1.00	.98	.82
[1] .25	.11	.25	.37	.48	.68	.83	.97	1.00
[1] .50	-.16	-.05	.06	.16	.34	.51	.71	.84
[1]1.00	-.26	-.19	-.11	-.03	.11	.24	.41	.55
[1]1.50	-.24	-.18	-.12	-.07	.04	.14	.28	.40
[1]2.50	-.15	-.11	-.07	-.03	.03	.10	.20	.28
[1]5.00	-.04	-.03	-.02	.01	.04	.07	.13	.17
[1]7.50	-.01	.01	.02	.02	.04	.07	.10	.12
[2] .10	.75	.62	.48	.30	-.15	-.75	-1.81	- -
[2] .25	.53	.38	.20	.01	-.48	-1.11	-2.16	- -
[2] .50	.41	.25	.09	-.10	-.52	-1.07	-1.98	- -
[2]1.00	.35	.21	.06	-.11	-.47	-.94	-1.66	-2.48
[2]1.50	.35	.21	.07	-.08	-.42	-.86	-1.52	-2.19
[2]2.50	.41	.28	.15	.01	-.30	-.64	-1.25	-1.99
[2]5.00	.55	.44	.34	.20	-.04	- 37	-.89	-1.51
[2]7.50	.63	.53	.43	.32	.10	-.18	-.65	-1.21

[1]Outside Contour
[2]Inside Contour

TABLE VI.- Continued.

$\alpha = 0^\circ$								
Distance aft of lip leading edge (in.)	Inlet-Velocity Ratio, V_1/V_o							
	0.54	0.61	0.67	0.74	0.87	1.00	1.20	1.40
[1]0.00	0.98	1.00	1.00	0.98	0.88	0.71	0.04	-1.03
[1] .10	.45	.58	.69	.78	.98	.99	1.00	.82
[1] .25	.05	.18	.31	.43	.64	.77	.96	1.00
[1] .50	-.24	-.13	-.02	.08	.29	.42	.68	.85
[1]1.00	-.35	-.28	-.18	-.12	.04	.15	.37	.53
[1]1.50	-.32	-.27	-.20	-.15	-.03	.06	.23	.38
[1]2.50	-.23	-.19	-.14	-.11	-.03	.03	.14	.24
[1]5.00	-.12	-.11	-.07	-.07	-.03	.01	.07	.12
[1]7.50	-.08	-.07	-.06	-.05	-.03	-.01	.03	.07
[2] .10	.75	.63	.50	.33	-.12	-.52	-1.77	- -
[2] .25	.53	.38	.21	.03	-.45	-.88	-2.13	- -
[2] .50	.41	.25	.10	-.08	-.51	-.88	-1.96	- -
[2]1.00	.35	.21	.07	-.10	-.47	-.78	-1.68	-2.69
[2]1.50	.36	.21	.07	-.08	-.43	-.72	-1.52	-2.55
[2]2.50	.41	.28	.15	.01	-.30	-.53	-1.25	-2.16
[2]5.00	.56	.44	.34	.21	-.04	-.26	-.88	-1.65
[2]7.50	.64	.53	.43	.33	.10	-.08	-.64	-1.33

[1]Outside Contour
[2]Inside Contour

TABLE VI.- Concluded.

$\alpha = 2^\circ$								
Distance aft of lip leading edge (in.)	Inlet-Velocity Ratio, V_1/V_o							
	0.54	0.61	0.67	0.74	0.87	1.00	1.20	1.40
[1]0.00	0.99	1.00	1.00	0.98	0.88	0.64	0.08	-0.98
[1] .10	.48	.58	.67	.75	.90	.98	.99	.82
[1] .25	.03	.16	.26	.38	.58	.76	.92	1.00
[1] .50	-.29	-.18	-.08	.02	.23	.40	.62	.81
[1]1.00	-.43	-.33	-.26	-.18	-.03	.12	.30	.48
[1]1.50	-.42	-.33	-.28	-.21	-.11	.01	.16	.31
[1]2.50	-.32	-.26	.23	-.18	-.11	-.03	.07	.18
[1]5.00	-.21	-.18	-.17	-.14	-.11	-.07	-.02	.04
[1]7.50	-.18	-.16	-.15	-.13	-.12	-.09	-.05	-.02
[2] .10	.66	.57	.47	.31	-.08	-.68	-1.73	- -
[2] .25	.41	.31	.18	.01	-.43	-1.05	-2.10	- -
[2] .50	.28	.18	.07	-.10	-.48	-1.03	-1.94	- -
[2]1.00	.26	.15	.03	-.11	-.44	-.92	-1.68	-2.69
[2]1.50	.28	.16	.05	-.09	-.40	-.84	-1.50	-2.55
[2]2.50	.37	.24	.13	.01	-.28	-.62	-1.23	-2.15
[2]5.00	.53	.41	.32	.21	-.02	-.34	-.86	-1.65
[2]7.50	.58	.46	.39	.30	.11	-.17	-.62	-1.34

[1]Outside Contour

[2]Inside Contour

TABLE VII.- THE VARIATION OF PRESSURE COEFFICIENT ALONG THE CENTER LINE OF THE LIP WITH ANGLE OF ATTACK AND INLET-VELOCITY RATIO FOR THE 7° RAMP WITH NO DIVERGENCE

$\alpha = -2^\circ$								
Distance aft of lip leading edge (in.)	Inlet-Velocity Ratio, V_1/V_o							
	0.54	0.61	0.67	0.74	0.87	1.00	1.20	1.40
[1]0.00	--	--	0.80	0.90	1.00	0.98	0.75	0.27
[1] .10	--	--	-.01	.19	.54	.78	.96	1.00
[1] .25	--	--	-.43	-.25	.11	.40	.68	.89
[1] .50	--	--	-.62	-.48	-.19	.06	.31	.55
[1]1.00	--	--	-.60	-.50	-.30	-.13	.06	.25
[1]1.50	--	--	-.49	-.42	-.28	-.15	-.01	.15
[1]2.50	--	--	-.28	-.27	-.17	-.09	.00	.11
[1]5.00	--	--	-.11	-.09	-.04	-.02	.02	.09
[1]7.50	--	--	-.05	-.04	-.01	.02	.03	.07
[2] .10	--	--	.91	.83	.53	.11	-.63	-1.63
[2] .25	--	--	.71	.57	.19	-.30	-1.11	-2.16
[2] .50	--	--	.51	.37	-.02	-.48	-1.21	-2.14
[2]1.00	--	--	.34	.20	-.15	-.58	-1.24	-2.03
[2]1.50	--	--	.26	.13	-.21	-.61	-1.24	-1.97
[2]2.50	--	--	.24	.11	-.20	-.57	-1.14	-1.73
[2]5.00	--	--	.30	.20	-.07	-.34	-.82	-1.39
[2]7.50	--	--	.42	.33	.10	-.18	-.59	-1.09

[1]Outside Contour
[2]Inside Contour

TABLE VII.- Continued.

$\alpha = 0^\circ$								
Distance aft of lip leading edge (in.)	Inlet-Velocity Ratio, V_1/V_o							
	0.54	0.61	0.67	0.74	0.87	1.00	1.20	1.40
[1]0.00	--	0.69	0.81	0.90	1.00	0.99	0.78	0.33
[1] .10	--	-.23	-.03	.14	.50	.74	.95	1.00
[1] .25	--	-.68	-.49	-.31	.06	.34	.64	.85
[1] .50	--	-.83	-.69	-.56	-.27	-.03	.26	.49
[1]1.00	--	-.75	-.66	-.57	-.38	-.23	-.01	.18
[1]1.50	--	-.63	-.55	-.49	-.35	-.23	-.07	.07
[1]2.50	--	-.36	-.35	-.34	-.24	-.18	-.06	.03
[1]5.00	--	-.19	-.17	-.15	-.12	-.10	-.03	.01
[1]7.50	--	-.13	-.12	-.10	-.07	-.07	-.02	.00
[2] .10	--	.96	.91	.83	.55	.14	-.60	-1.58
[2] .25	--	.78	.69	.58	.20	-.29	-1.10	-2.12
[2] .50	--	.58	.49	.36	-.02	-.47	-1.22	-2.13
[2]1.00	--	.40	.31	.20	-.16	-.58	-1.25	-2.04
[2]1.50	--	.31	.23	.12	-.23	-.62	-1.26	-1.99
[2]2.50	--	.28	.20	.11	-.22	-.58	-1.16	-1.75
[2]5.00	--	.34	.28	.19	-.08	-.35	-.83	-1.40
[2]7.50	--	.45	.40	.32	.08	-.18	-.60	-1.10

[1]Outside Contour
[2]Inside Contour

TABLE VII.– Concluded.

$\alpha = 2^\circ$								
Distance aft of lip leading edge (in.)	Inlet-Velocity Ratio, V_1/V_o							
	0.54	0.61	0.67	0.74	0.87	1.00	1.20	1.40
[1]0.00	– –	0.71	0.82	0.91	1.00	0.98	0.77	0.35
[1] .10	– –	–.23	–.03	.13	.47	.72	.93	.99
[1] .25	– –	–.70	–.50	–.34	.01	.30	.60	.81
[1] .50	– –	–.88	–.72	–.60	–.33	–.07	.21	.43
[1]1.00	– –	–.82	–.72	–.64	–.45	–.28	–.06	.11
[1]1.50	– –	–.61	–.61	–.55	–.43	–.29	–.14	.00
[1]2.50	– –	–.46	–.44	–.41	–.32	–.22	–.13	–.04
[1]5.00	– –	–.27	–.24	–.22	–.20	–.16	–.12	–.07
[1]7.50	– –	–.22	–.19	–.19	–.16	–.14	–.12	–.09
[2]0.10	– –	.93	.88	.80	.52	.13	–.63	–1.53
[2] .25	– –	.73	..64	.52	.16	–.30	–1.13	–2.10
[2] .50	– –	.52	.43	.30	–.05	–.49	–1.25	–2.11
[2]1.00	– –	.34	.26	.14	–.19	–.59	–1.26	–2.02
[2]1.50	– –	.26	.18	.08	–.26	–.64	–1.28	–1.98
[2]2.50	– –	.22	.16	.05	–.24	–.58	–1.17	–1.73
[2]5.00	– –	.30	.24	.16	–.09	–.34	–.84	–1.37
[2]7.50	– –	.42	.37	.29	.08	–.17	–.61	–1.07

[1]Outside Contour

[2]Inside Contour

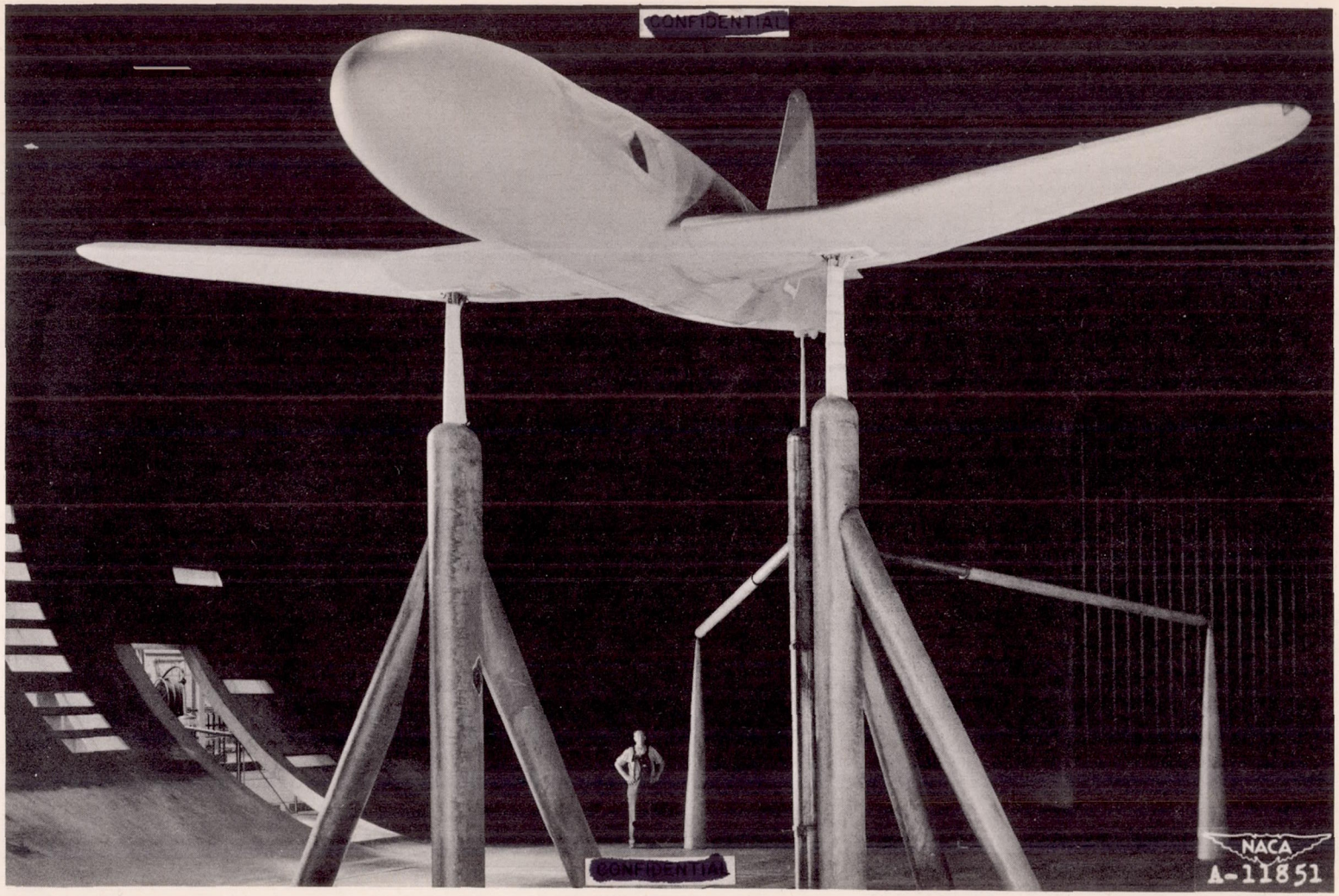

Figure 1.- General view of the full-scale model with an NACA submerged entrance.

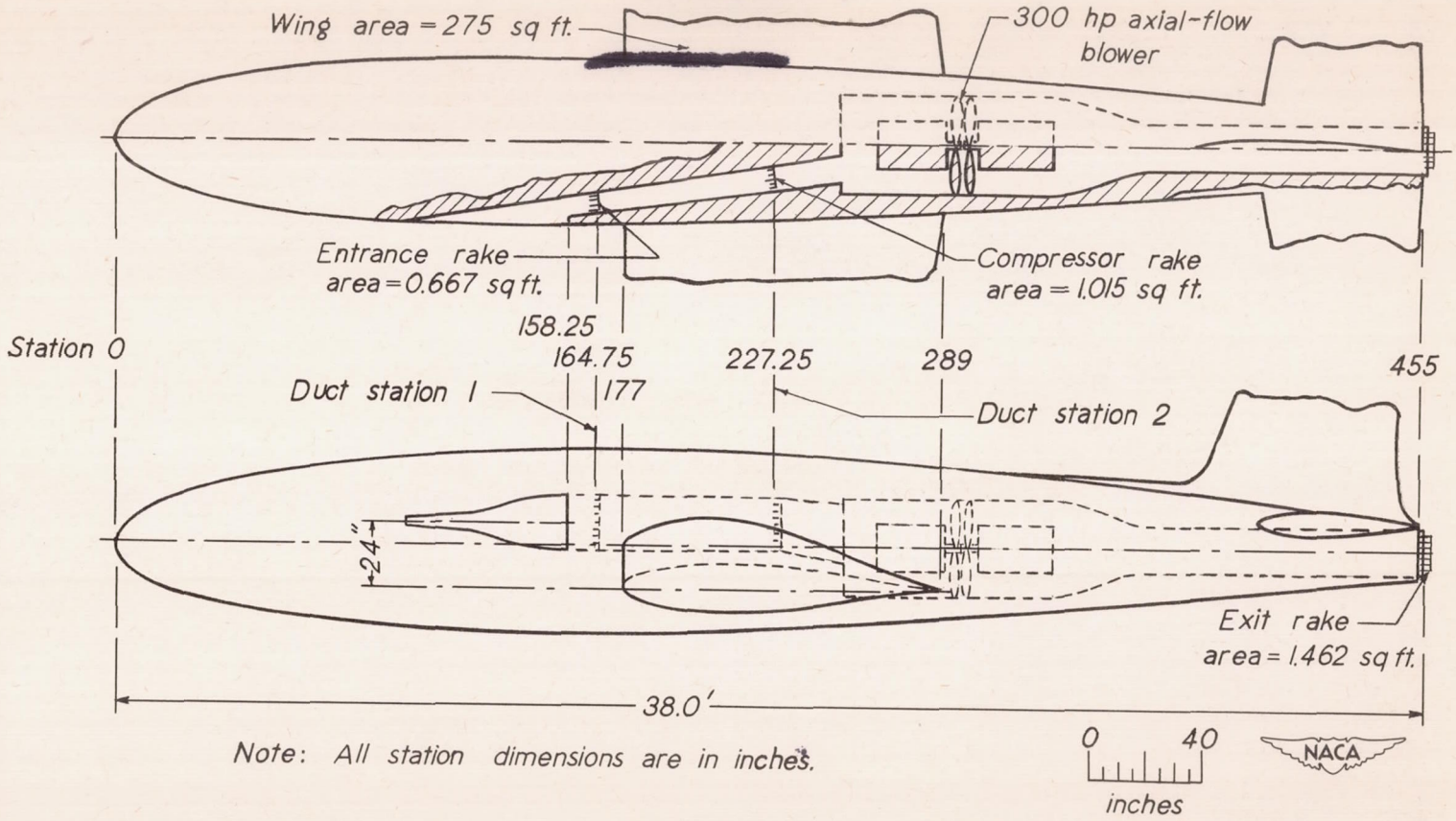

Figure 2.- Schematic drawing showing general arrangement of full-scale model of fighter airplane with an NACA submerged air intake installed.

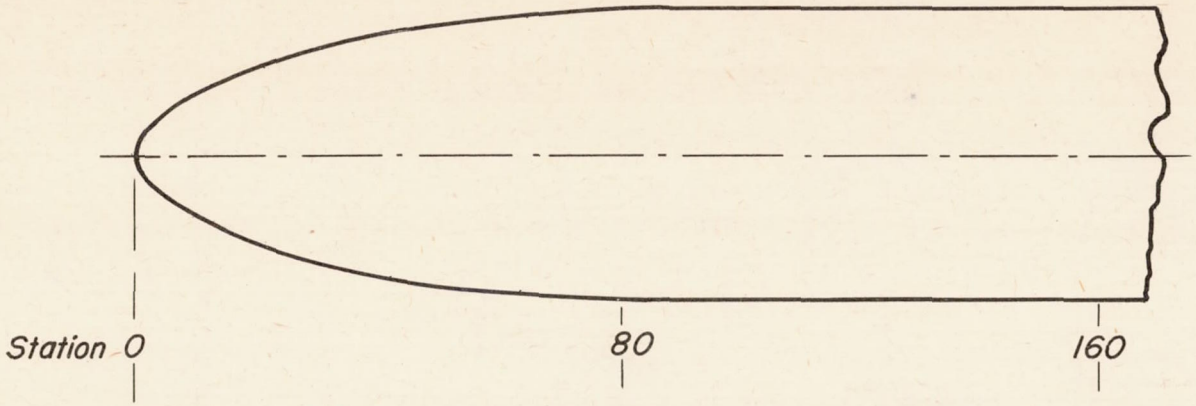

Station	Radius
0	0
5.22	8.18
10.44	12.28
20.89	17.67
41.78	23.51
62.67	27.02
83.56	28.50
160.00	28.50

All dimensions are in inches.

Figure 3.- Fuselage nose coordinates.

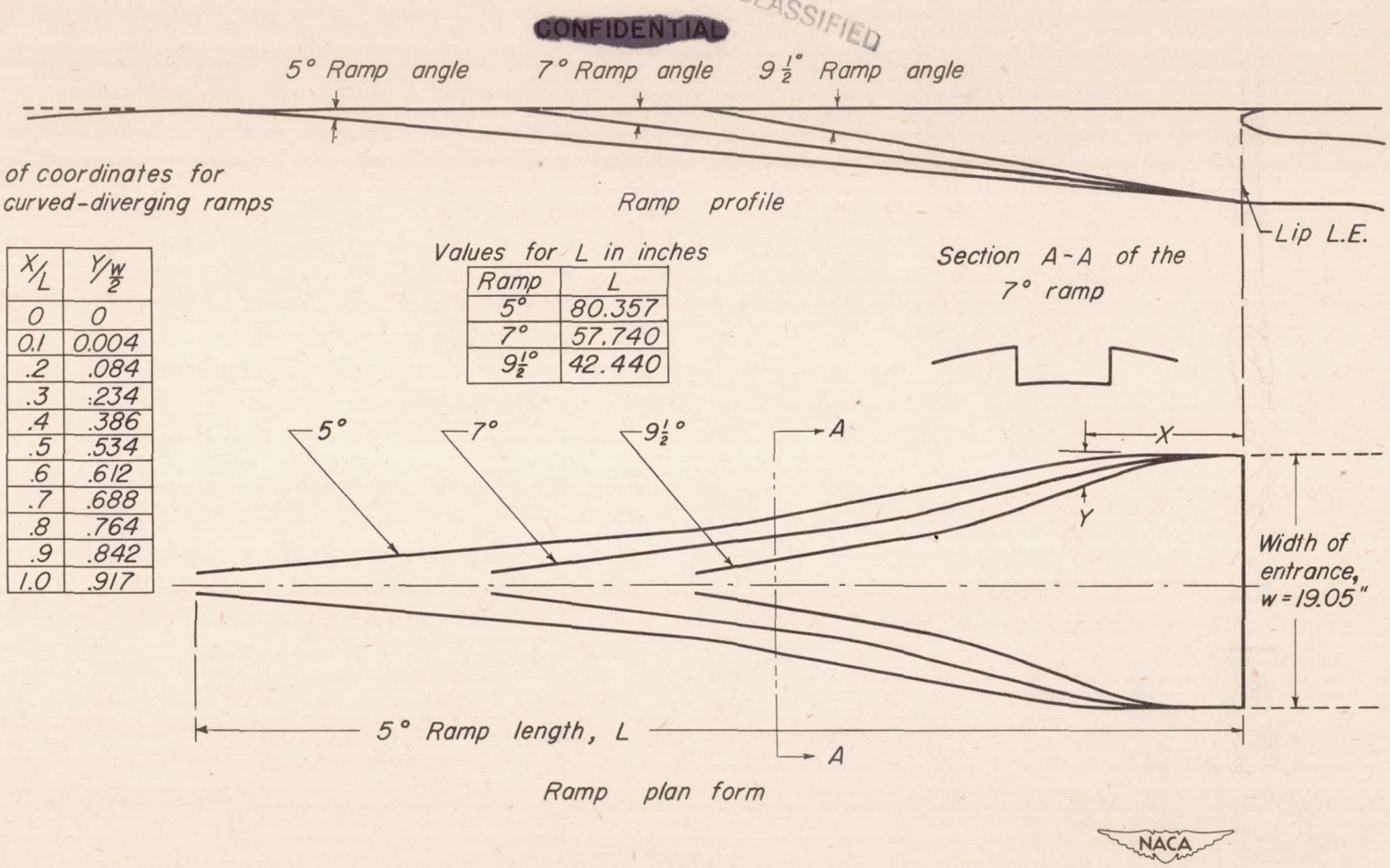

Table of coordinates for standard curved-diverging ramps

X/L	$Y/\frac{w}{2}$
0	0
0.1	0.004
.2	.084
.3	.234
.4	.386
.5	.534
.6	.612
.7	.688
.8	.764
.9	.842
1.0	.917

Values for L in inches

Ramp	L
5°	80.357
7°	57.740
9½°	42.440

Figure 4.- Coordinates of the standard curved-diverging ramp configurations tested on the full-scale model.

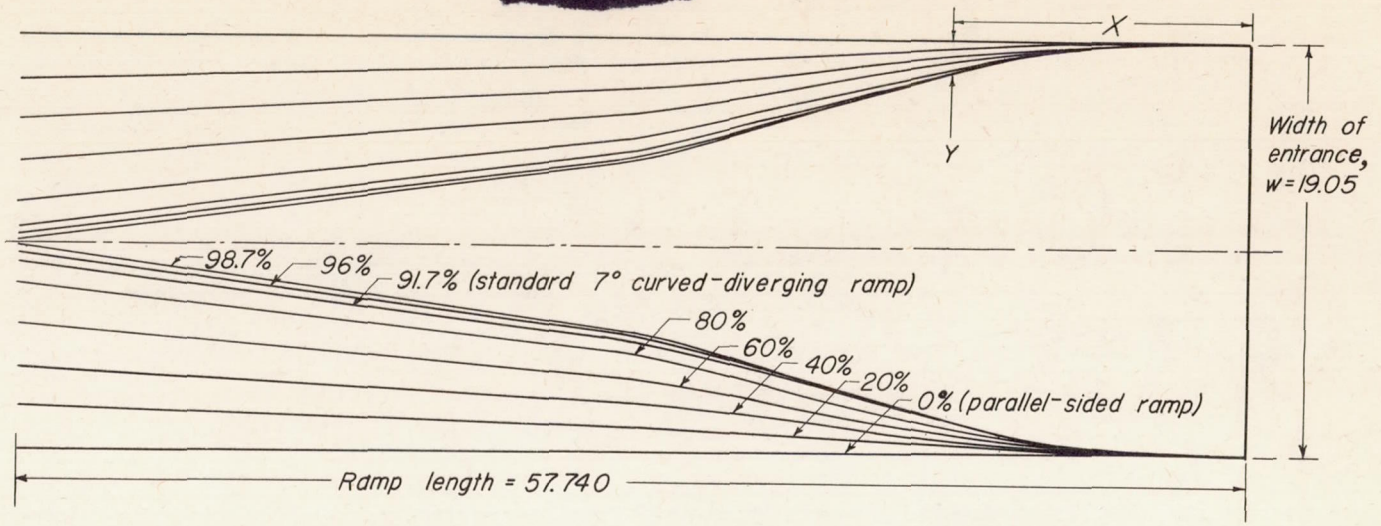

Table of coordinates for the 7° variable curved-diverging ramps

X/L	$Y/\frac{w}{2}$							
	0%	20%	40%	60%	80%	91.7%	96%	98.7%
0.0	0	0	0	0	0	0	0	0
.1	0	0.001	0.002	0.002	0.003	0.004	0.004	0.004
.2	0	.018	.037	.055	.074	.084	.088	.092
.3	0	.051	.102	.153	.204	.234	.245	.252
.4	0	.084	.168	.253	.337	.386	.404	.415
.5	0	.116	.233	.349	.466	.534	.559	.574
↓	↓	↑ Linear ↓	↑ Linear ↓	↑ Linear ↓	↑ Linear ↓	↑ Linear ↓	↑ Linear ↓	↑ Linear ↓
1.0	0	.200	.400	.600	.800	.917	.960	.987

NACA

Figure 5.- The coordinates of the various 7° ramp plan forms tested on the full-scale model.

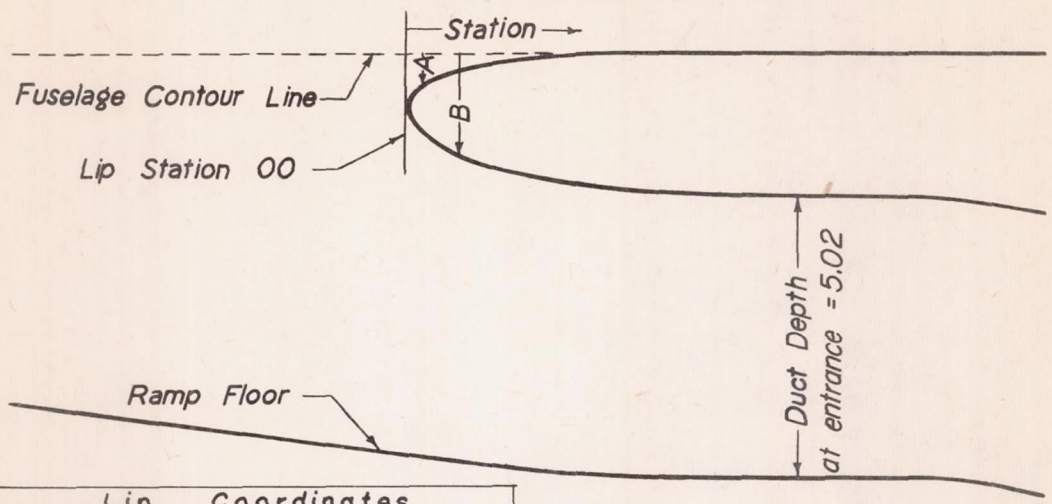

Lip Coordinates					
Stat.	A	B	Stat.	A	B
0.000	0.994	0.994	4.392	0.009	2.460
0.625	0.379	1.682	5.020	0.000	2.480
1.255	0.215	1.945	6.750	0.000	2.510
1.882	0.125	2.115	7.500	0.000	2.515
2.510	0.075	2.240	8.250	0.000	2.530
3.130	0.042	2.338	9.000	0.000	2.550
3.765	0.021	2.215	L.E. Rad. = 0.472		

All dimensions are in inches

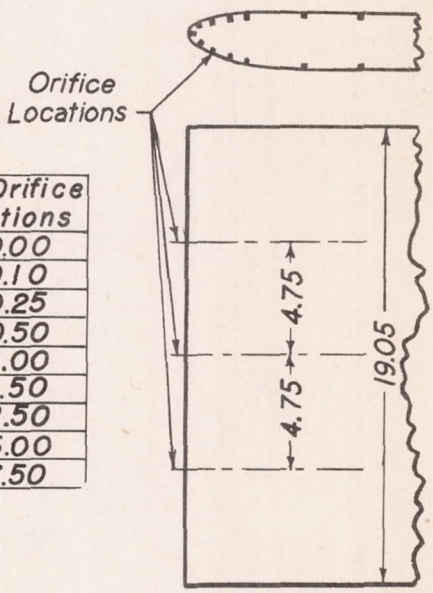

Lip Orifice Stations
0.00
0.10
0.25
0.50
1.00
1.50
2.50
5.00
7.50

NACA

Figure 6.- Details of the submerged lip.

[redacted]

[redacted]

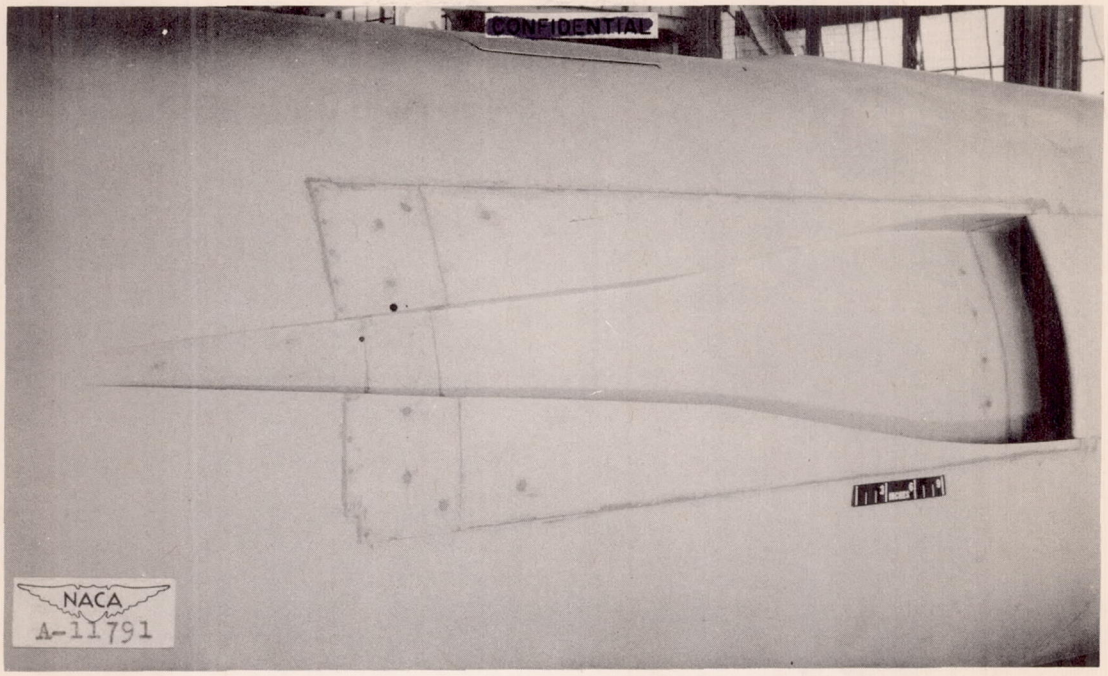

(a) 5° ramp, standard divergence.

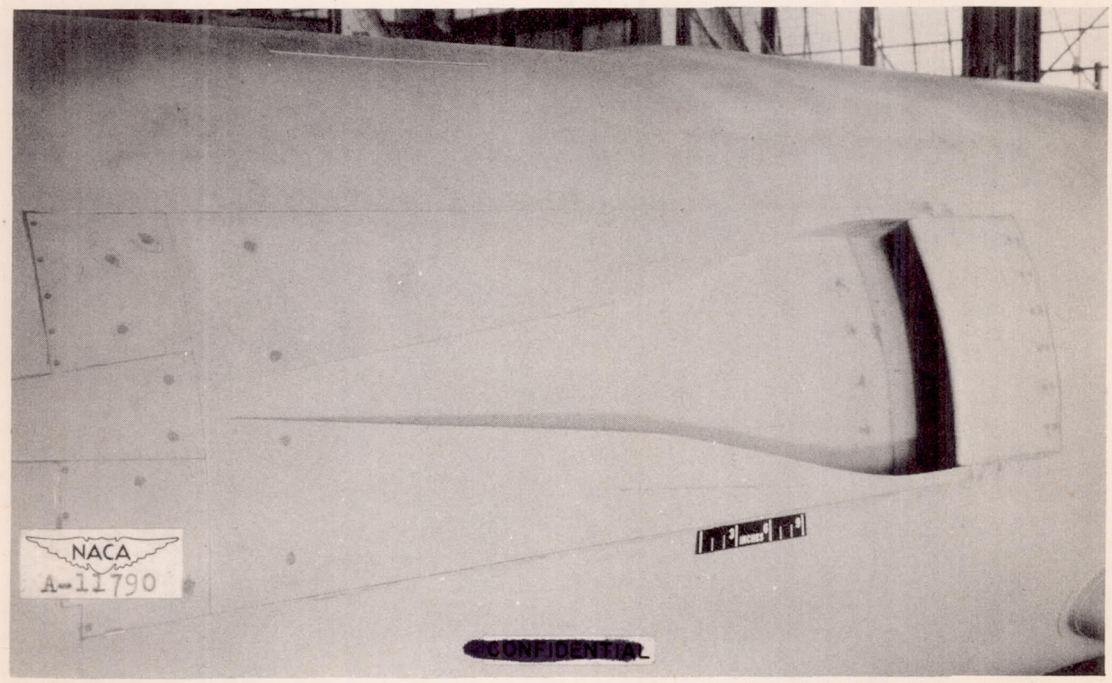

(b) 7° ramp, standard divergence.

Figure 7.- Views of several inlet configurations tested on the model of a fighter airplane.

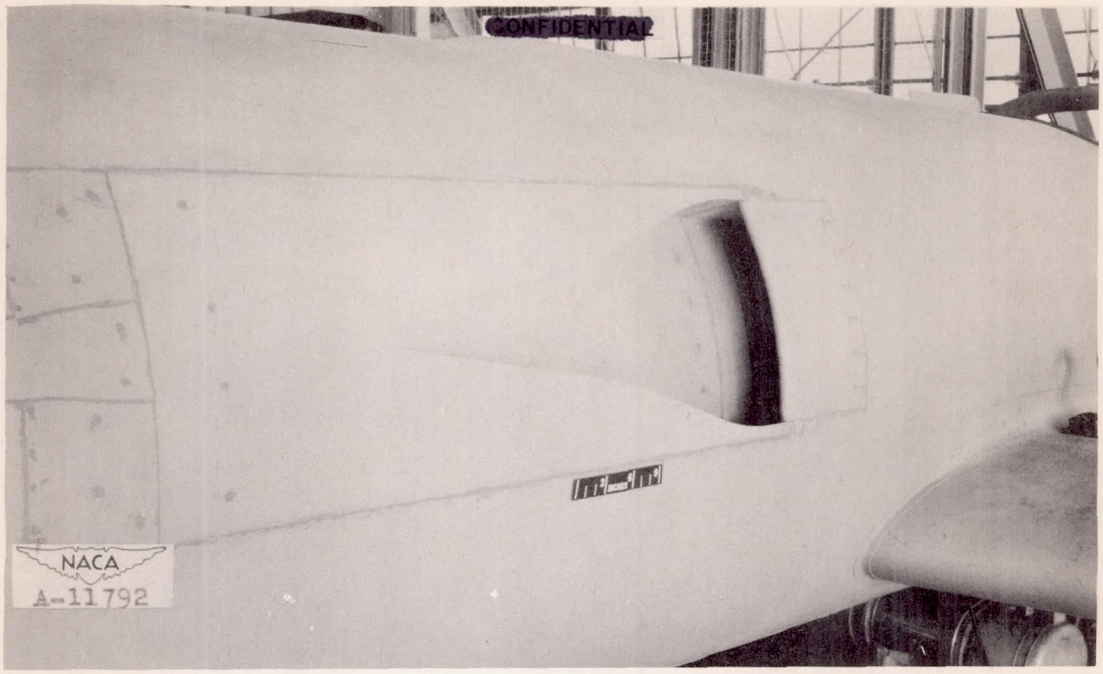

(c) $9\frac{1}{2}^{\circ}$ ramp, standard divergence.

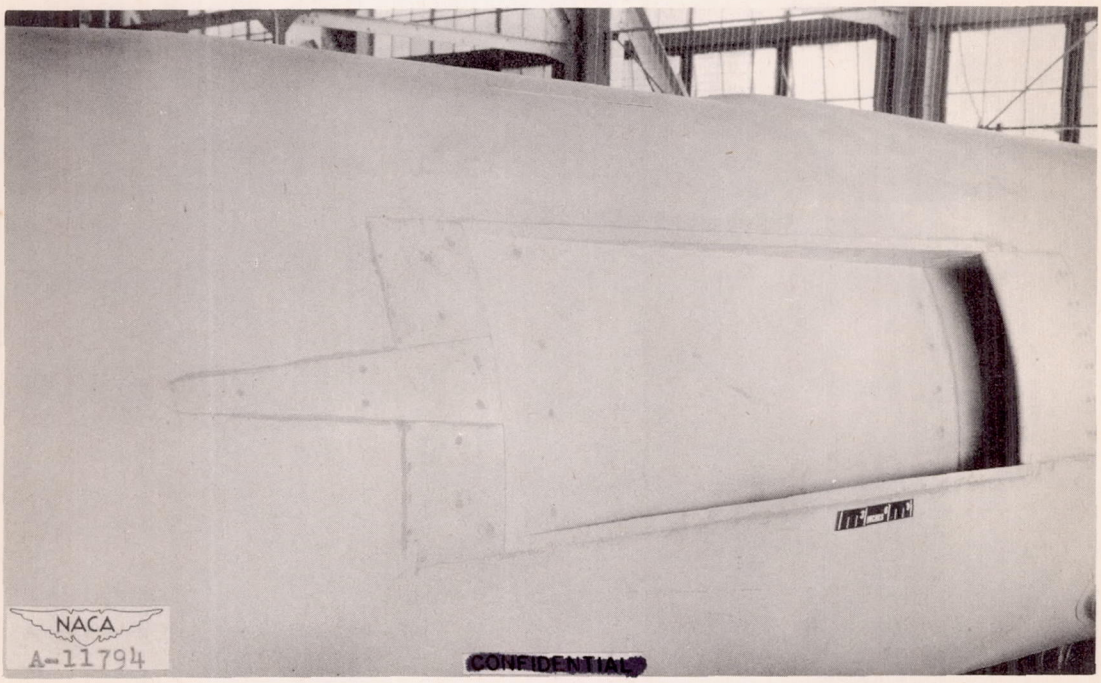

(d) 7° ramp, no divergence.

Figure 7.- Concluded

[redacted]

UNCLASSIFIED

[redacted]

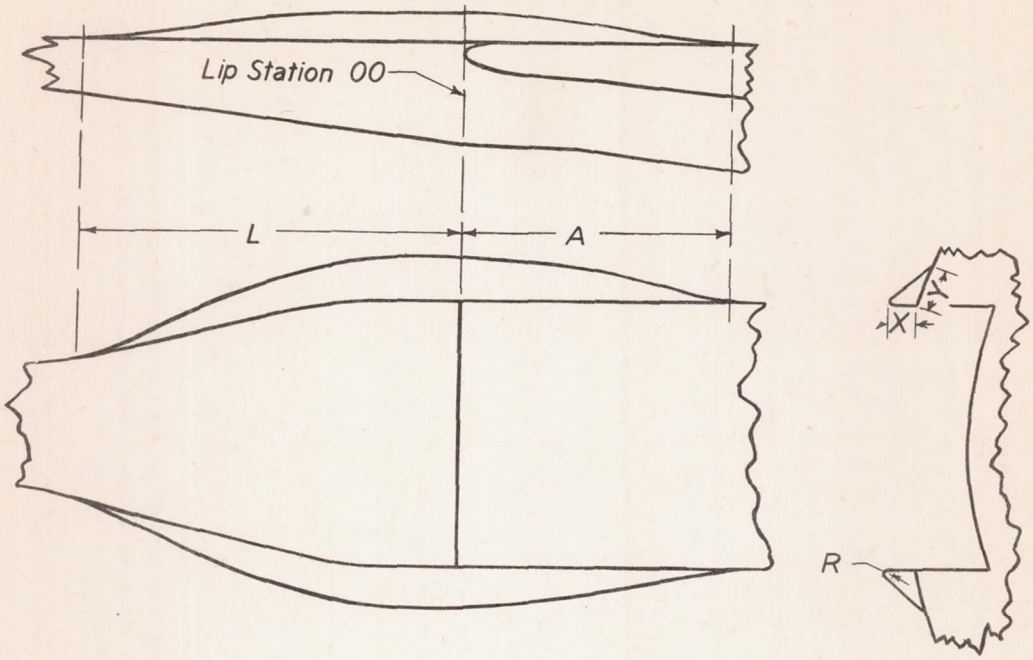

Deflector Coordinates					
Forward of Stat. 00			Aft of Stat. 00		
% L	X	Y	% A	X	Y
0	1.91	2.78	0	1.91	2.78
10	1.97	2.87	10	1.88	2.72
20	1.94	2.83	20	1.78	2.59
30	1.88	2.72	30	1.59	2.31
40	1.78	2.58	40	1.40	2.02
50	1.52	2.20	50	1.19	1.73
60	1.26	1.83	60	.90	1.30
70	.92	1.34	70	.66	.60
80	.59	.79	80	.38	.54
90	.22	.32	90	.14	.20
100	.00	.00	100	.00	.00

Ramp	L	A
7°	28.87	21.65
9½°	21.21	21.65

$R = 0.15\,Y$

All dimensions are in inches

Figure 8.- Coordinates of deflectors tested.

(a) 7° ramp, standard divergence.

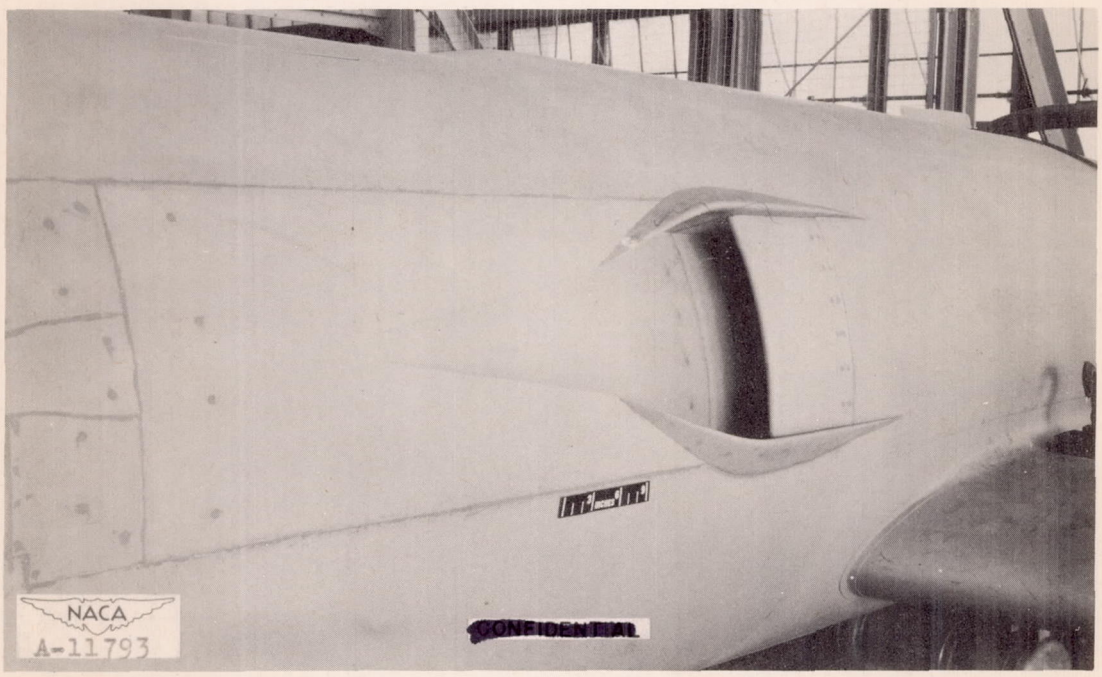

(b) $9\frac{1}{2}^{\circ}$ ramp, standard divergence.

Figure 9.- View of deflectors installed on two different NACA submerged entrances.

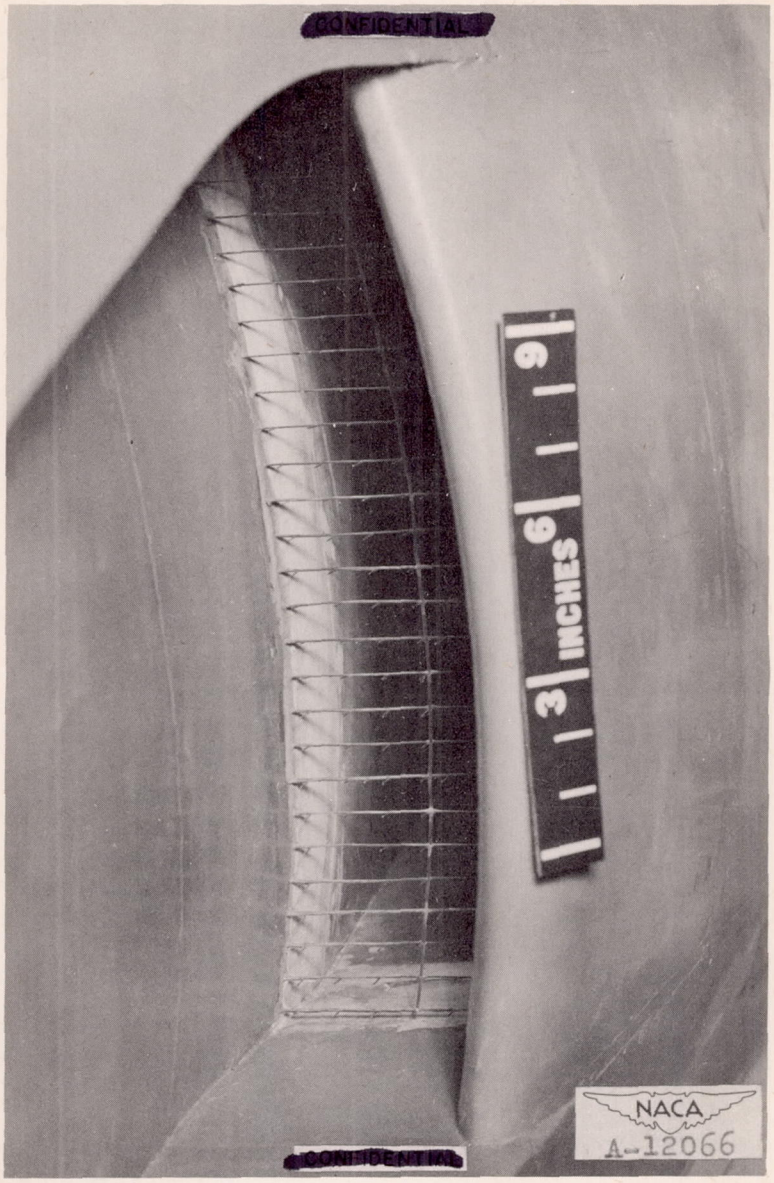

Figure 10.- Pressure rake at the submerged entrance (duct station 1).

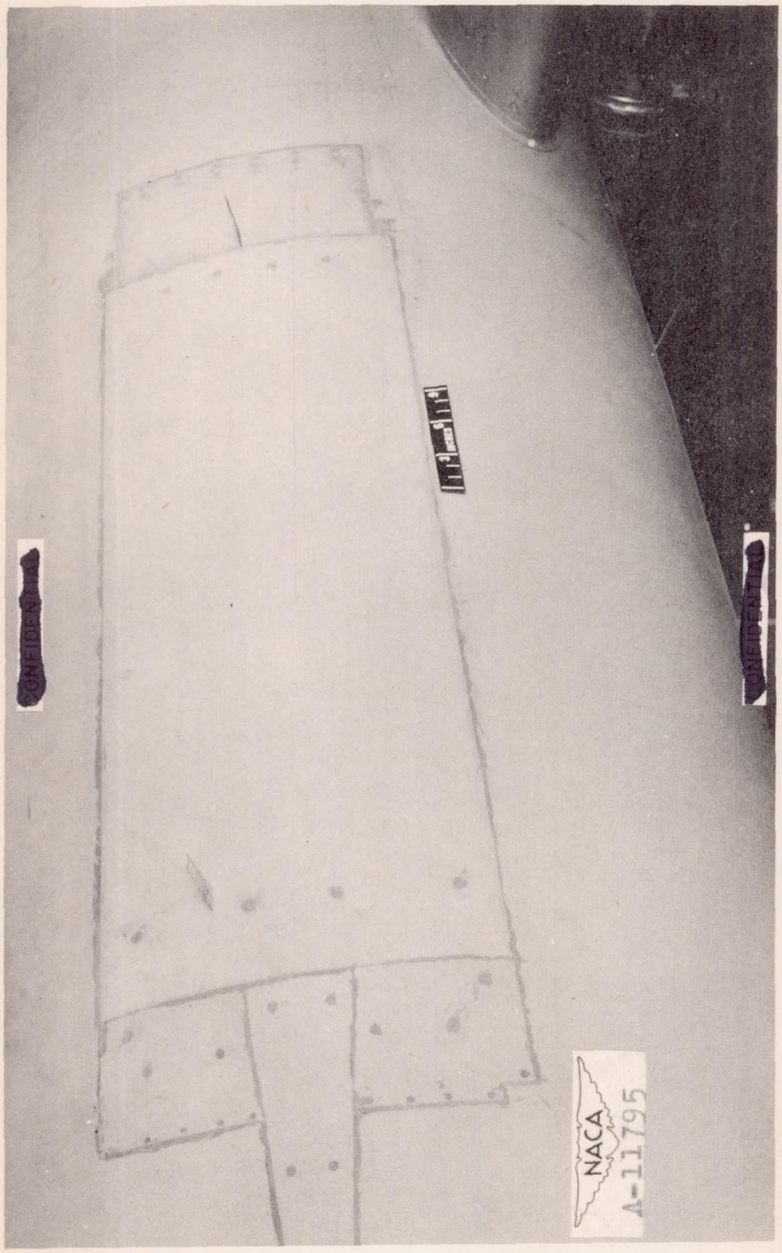

Figure 11.- View of basic fuselage and boundary-layer rakes.

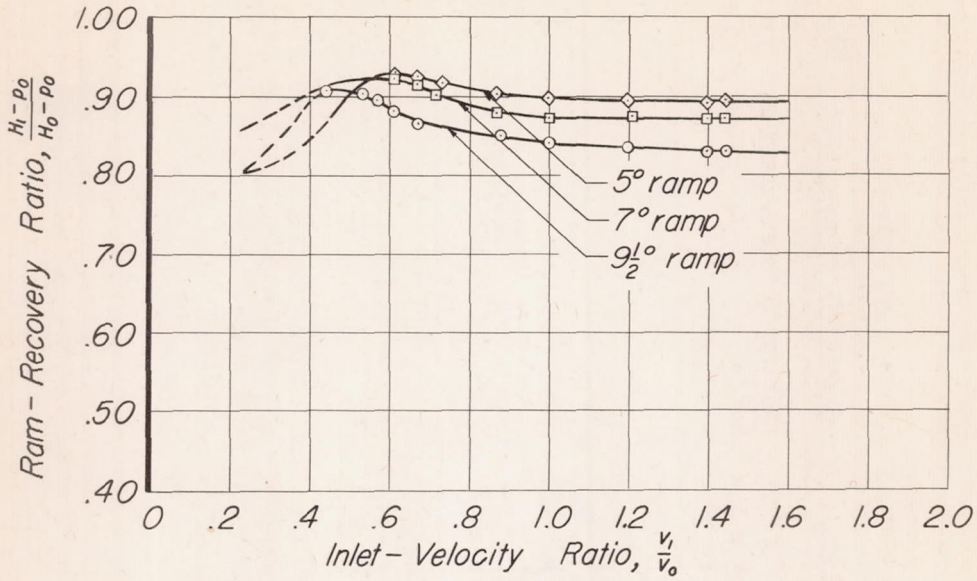

(a) Standard curved-diverging ramps

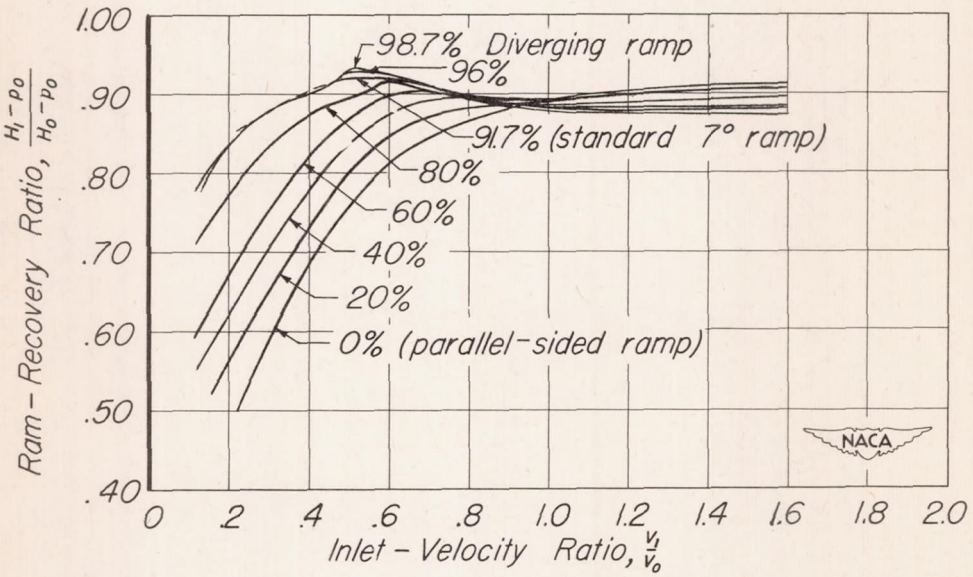

(b) 7° variable curved-diverging ramps

Figure 12.- The variation of entrance ram-recovery ratio with inlet-velocity ratio for several entrance configurations, $\alpha = 2°$.

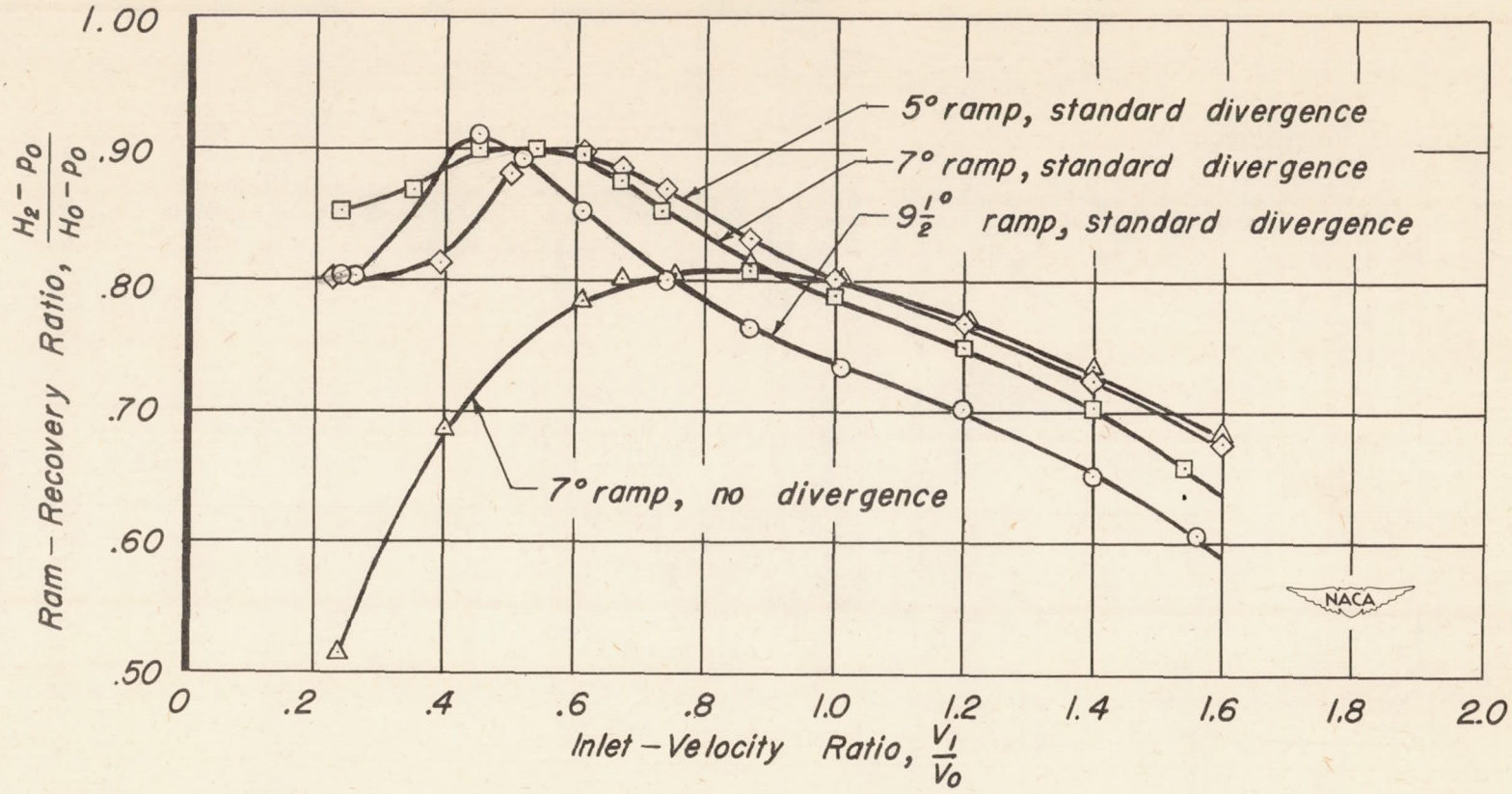

Figure 13.- The variation of ram-recovery ratio, measured after diffusion, with inlet-velocity ratio for several entrance configurations, $\alpha = -2°$.

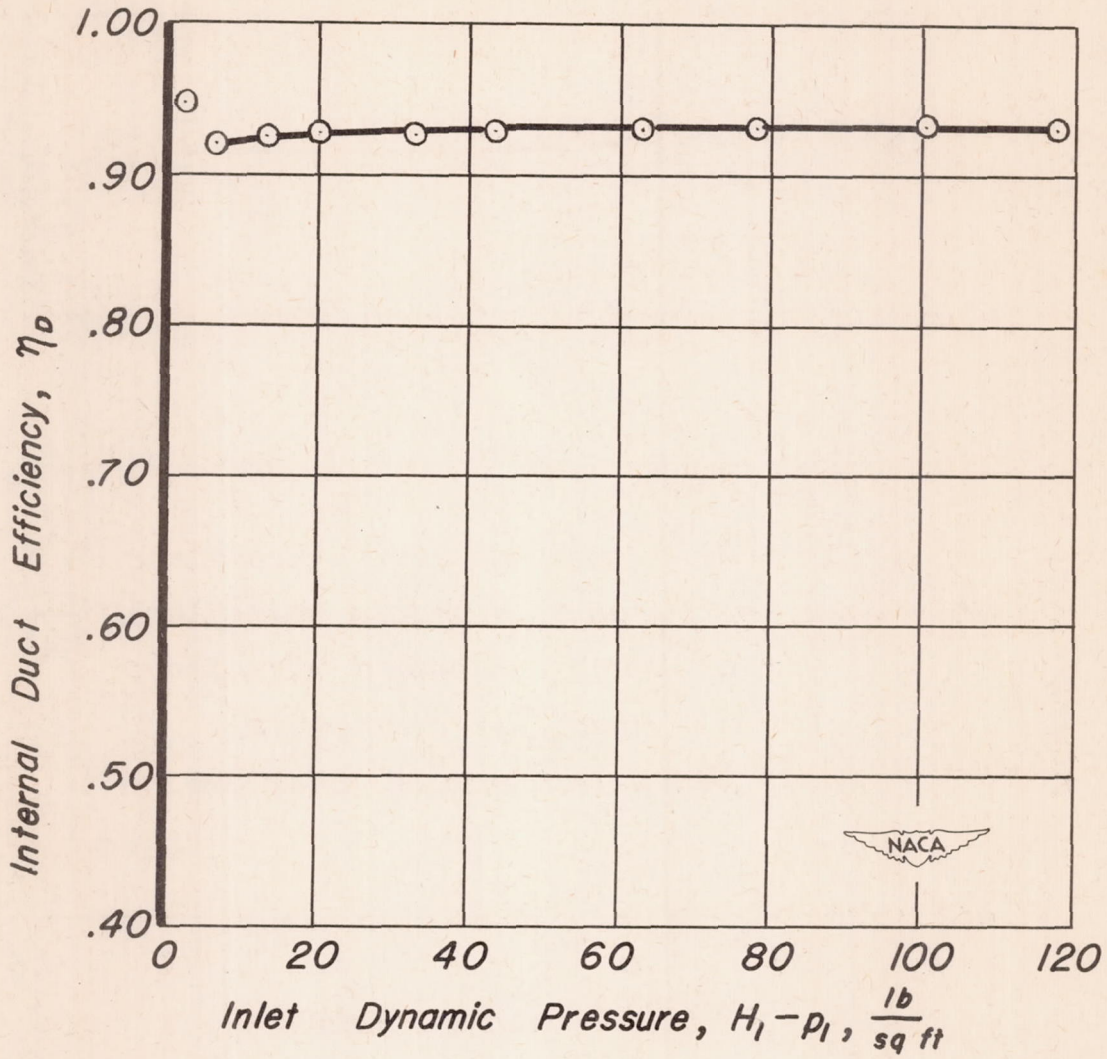

Figure. 14.- Internal duct efficiency determined from a bench test with entrance nozzle installed.

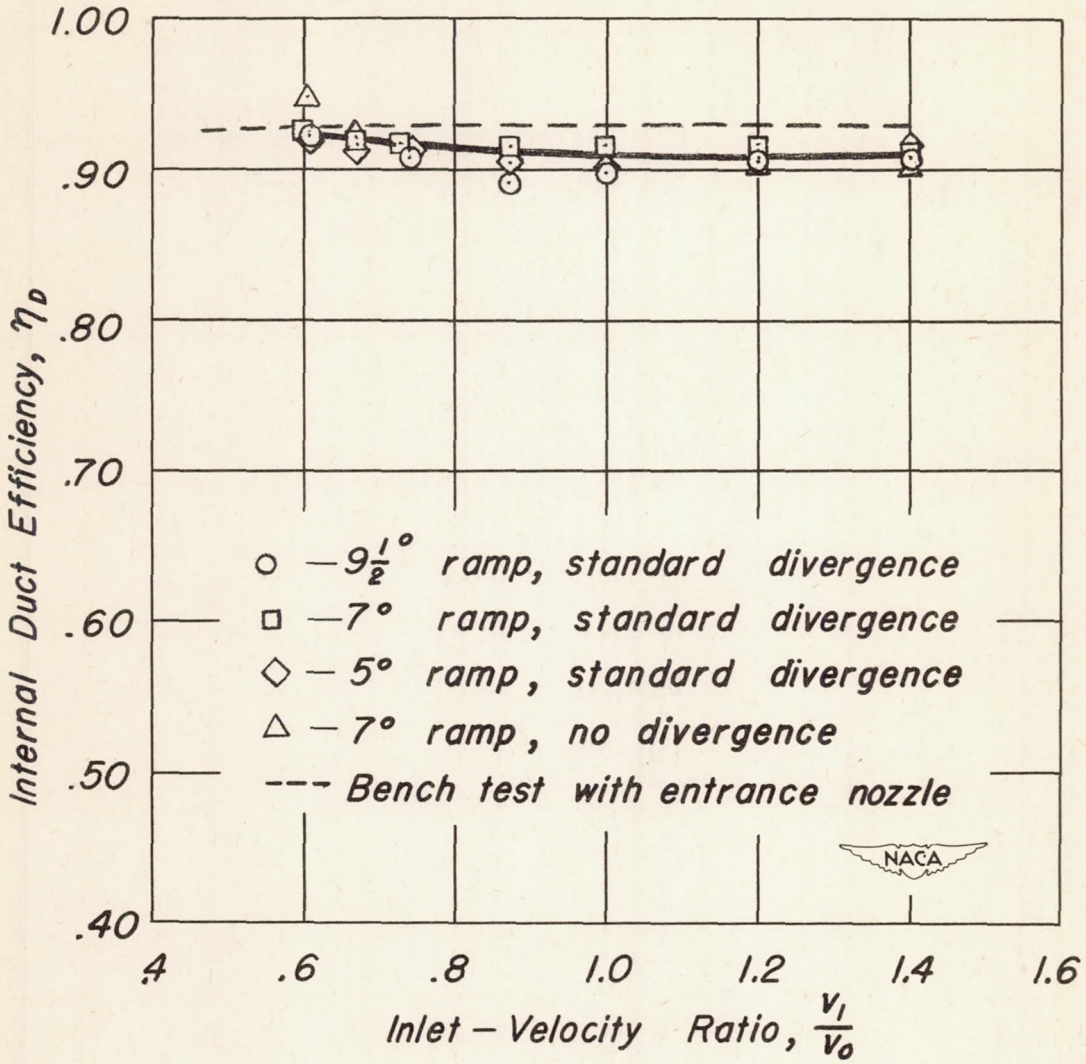

Figure 15.- Comparison of experimental duct efficiencies for various entrance configurations, α=-2°.

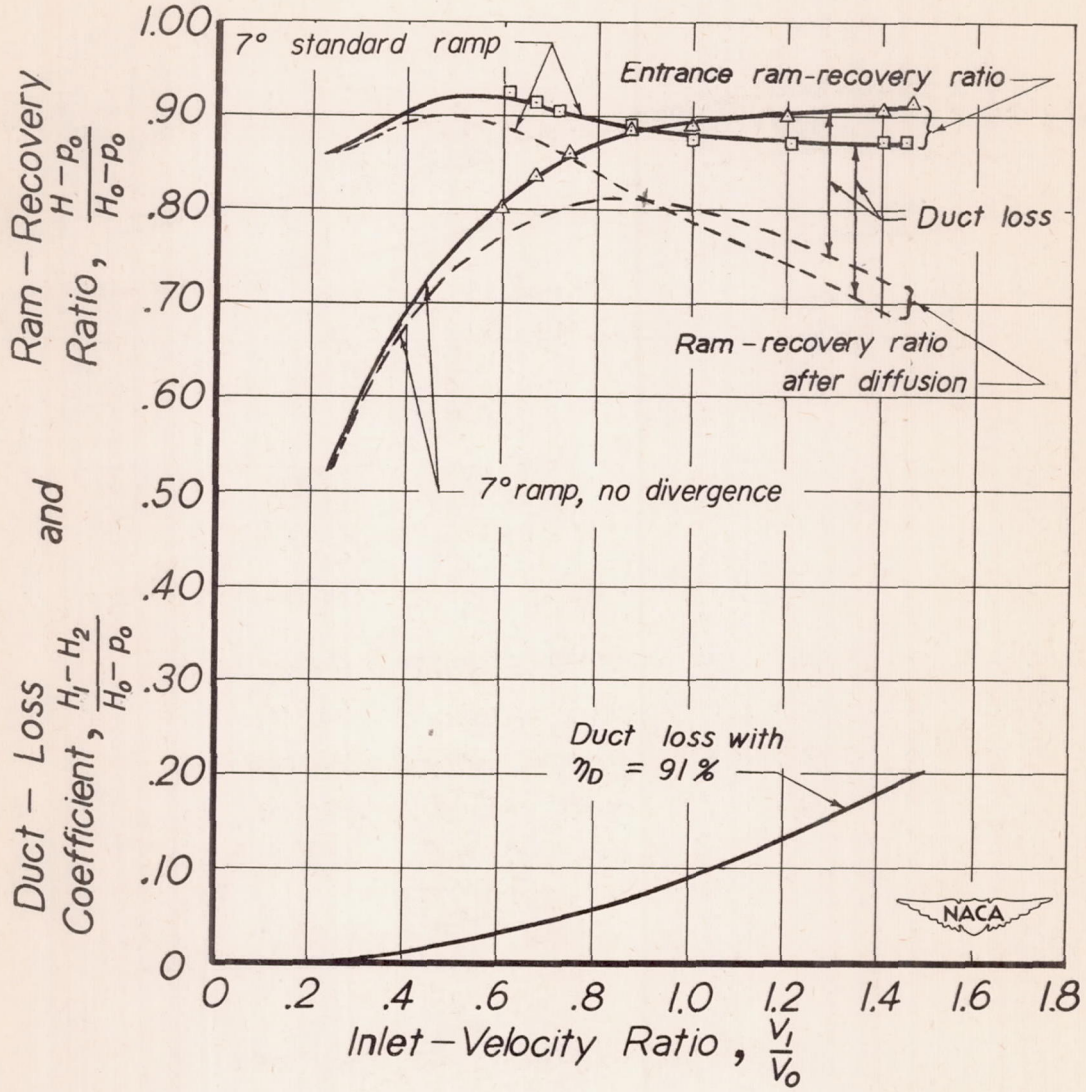

Figure 16.- Effect of duct loss on ram-recovery ratio after diffusion, α=-2°.

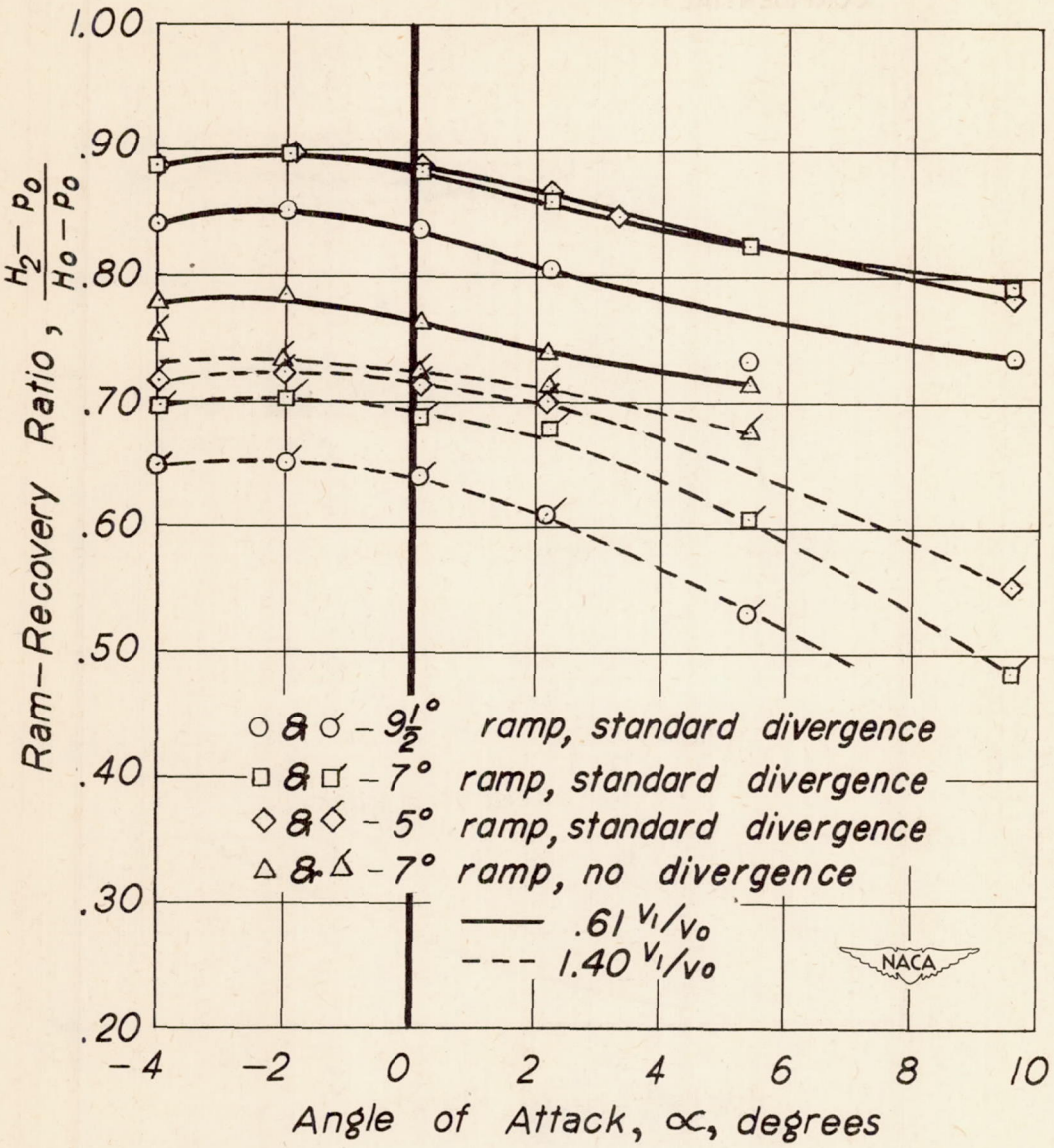

Figure 17.- Variation of ram-recovery ratio, measured after diffusion, with angle of attack for various entrance configurations.

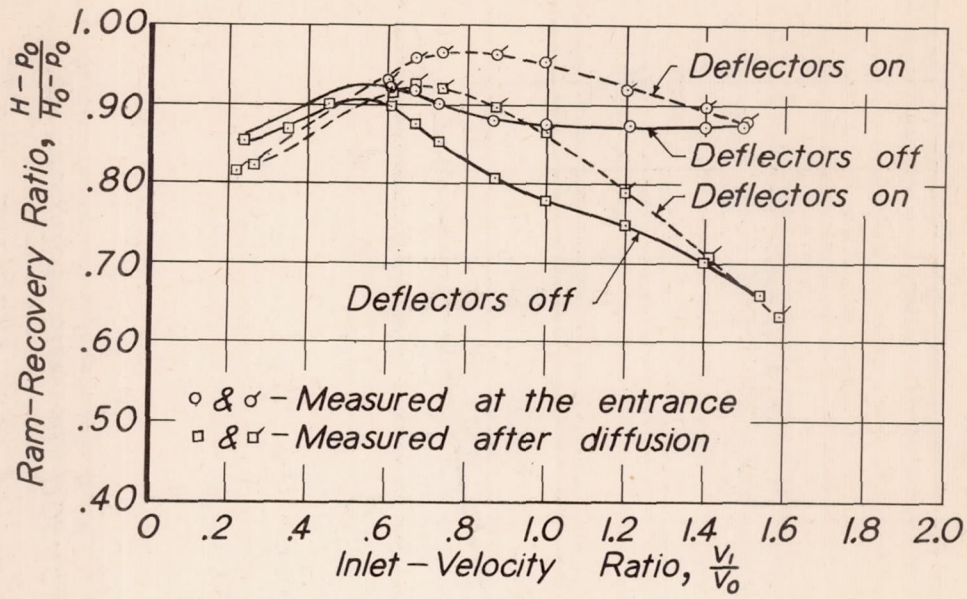

(a) 7° ramp, standard divergence

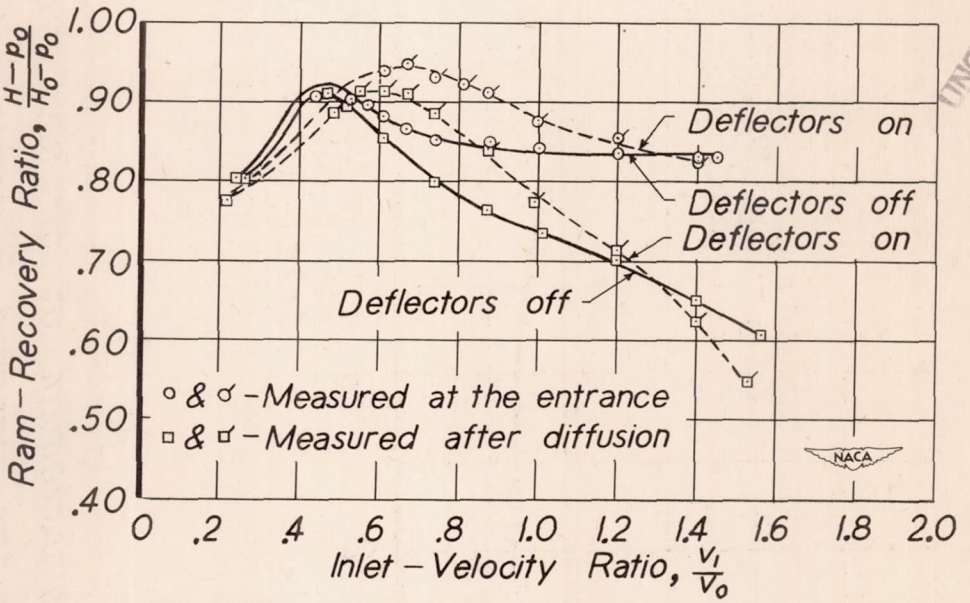

(b) 9½° ramp, standard divergence.

Figure 18.- The effect of deflectors on ram-recovery ratio, $\alpha = -2°$.

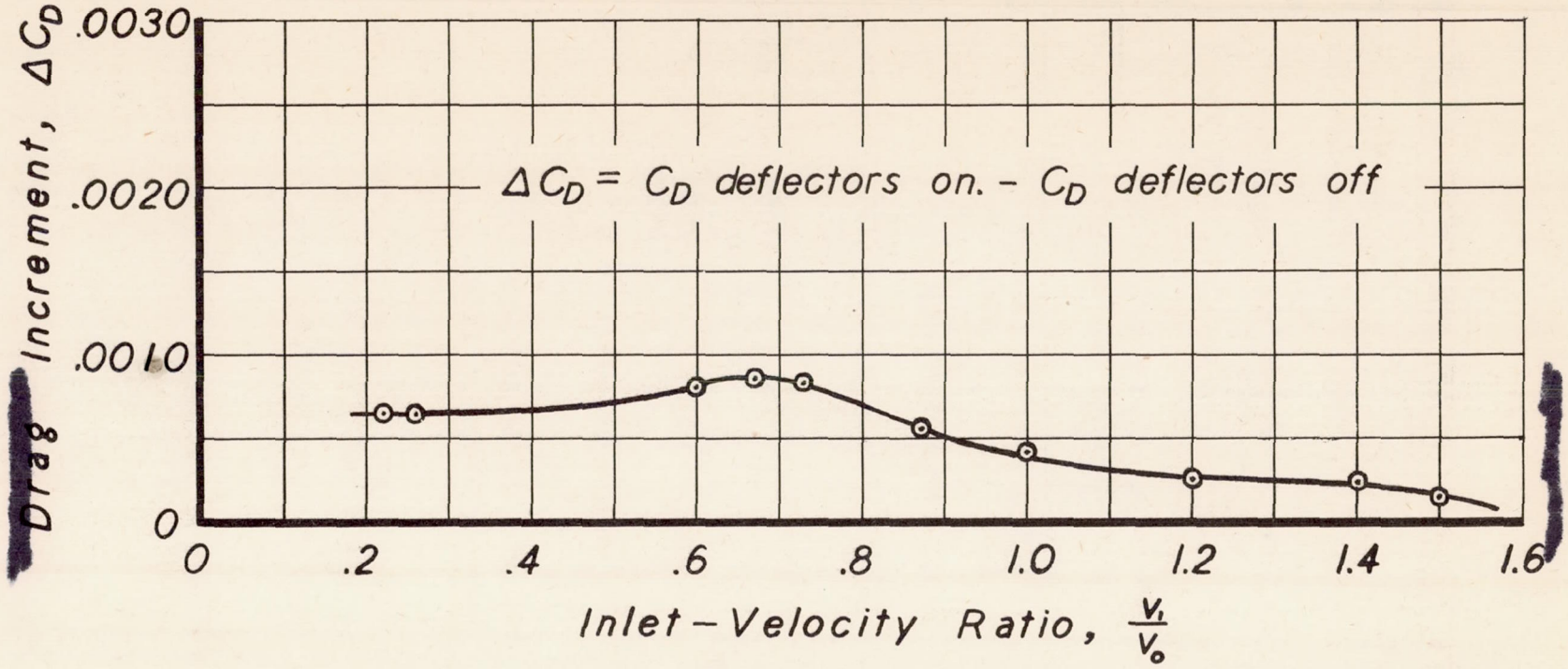

Figure 19.- The increment of airplane drag caused by the addition of deflectors to the standard 7° ramp on one side of the fuselage, α=2°.

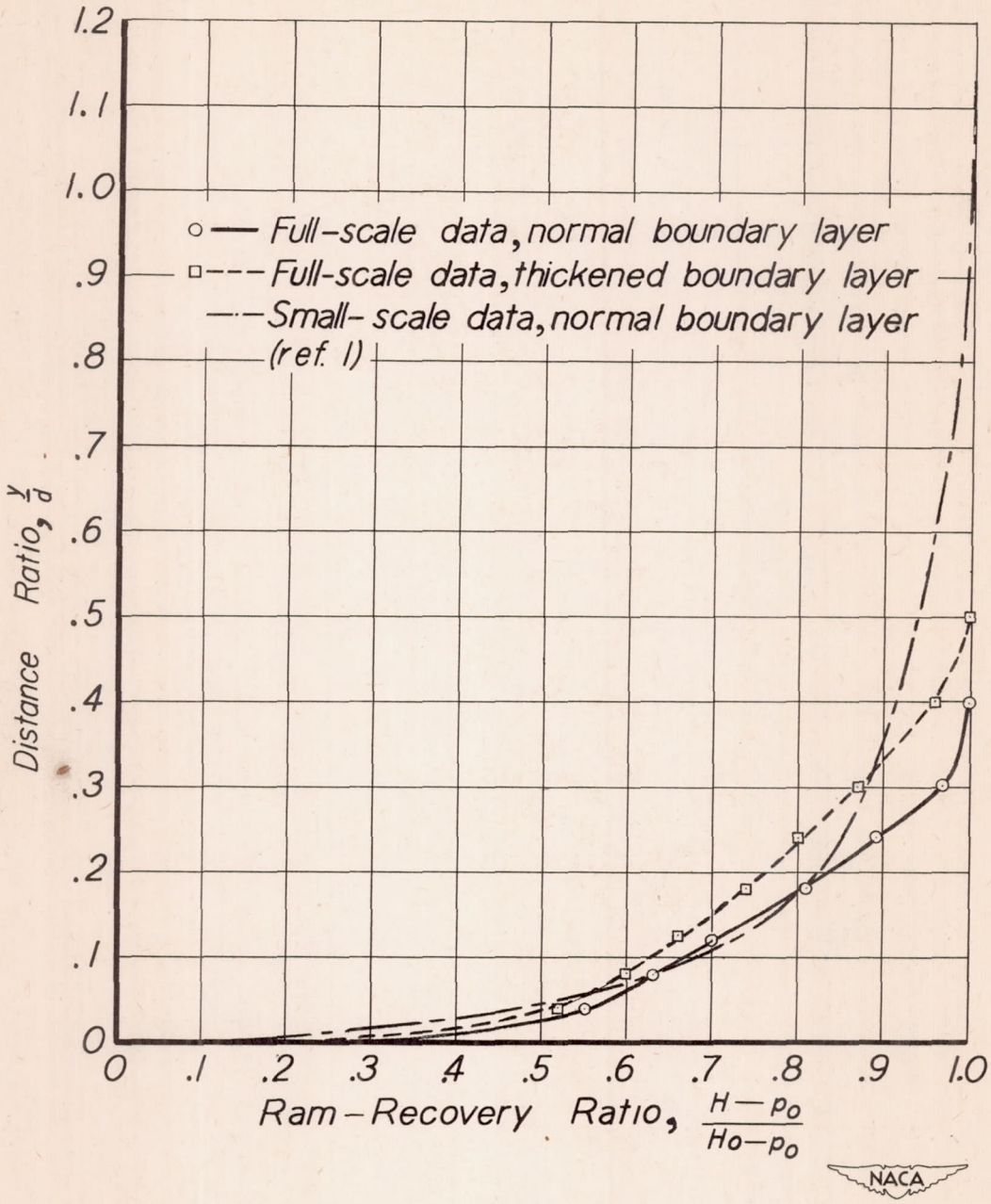

Figure 20.- Comparison of full-scale normal and thickened boundary layer with the small-scale boundary layer measured on the basic fuselage at the entrance station, $\alpha = 2°$.

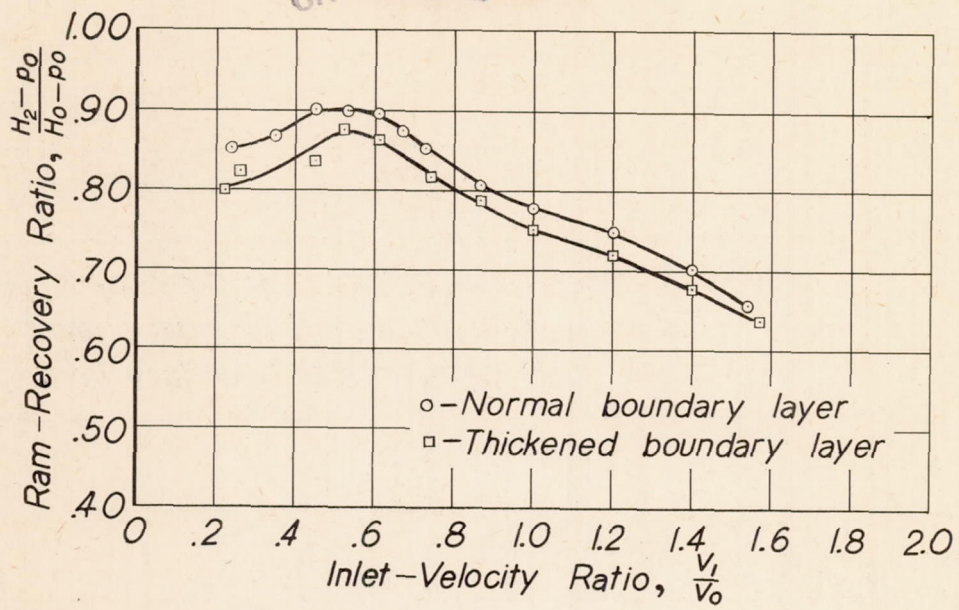

(a) 7° ramp, standard divergence

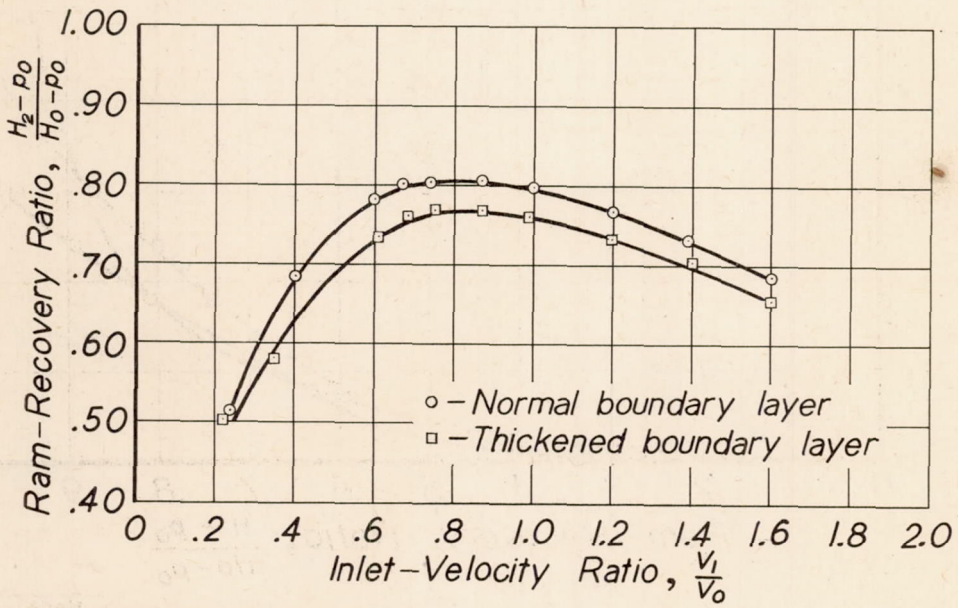

(b) 7° ramp, no divergence.

NACA

Figure 21.- The variation of ram-recovery ratio, measured after diffusion, with inlet-velocity ratio for two boundary-layer conditions, $\alpha = 2°$.

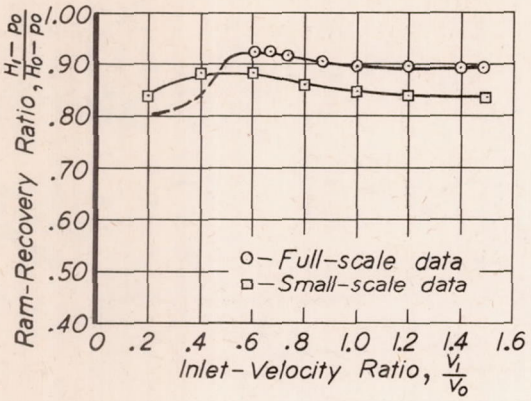

(a) 5° ramp, standard divergence.

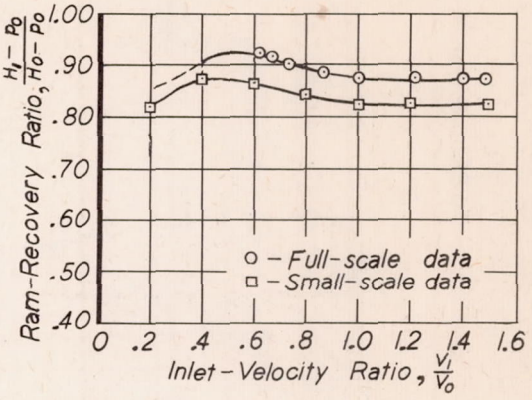

(b) 7° ramp, standard divergence.

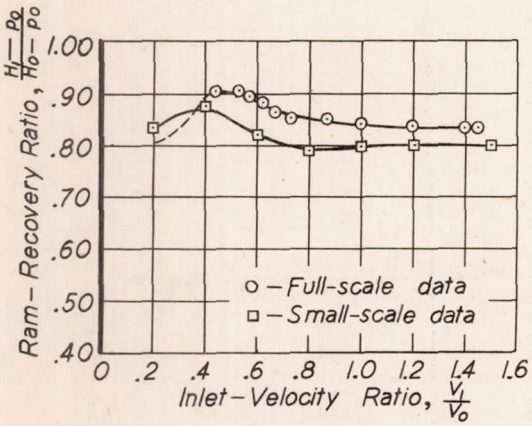

(c) $9\frac{1}{2}$° ramp, standard divergence.

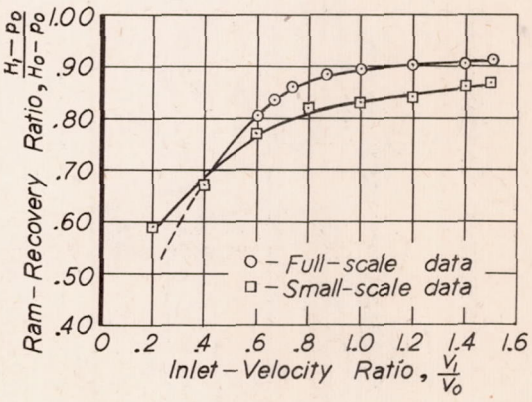

(d) 7° ramp, no divergence.

NACA

Figure 22.– Comparison of the entrance ram-recovery ratio of the full-scale model at $\alpha = -2°$ with that of the small-scale model (reference 1).

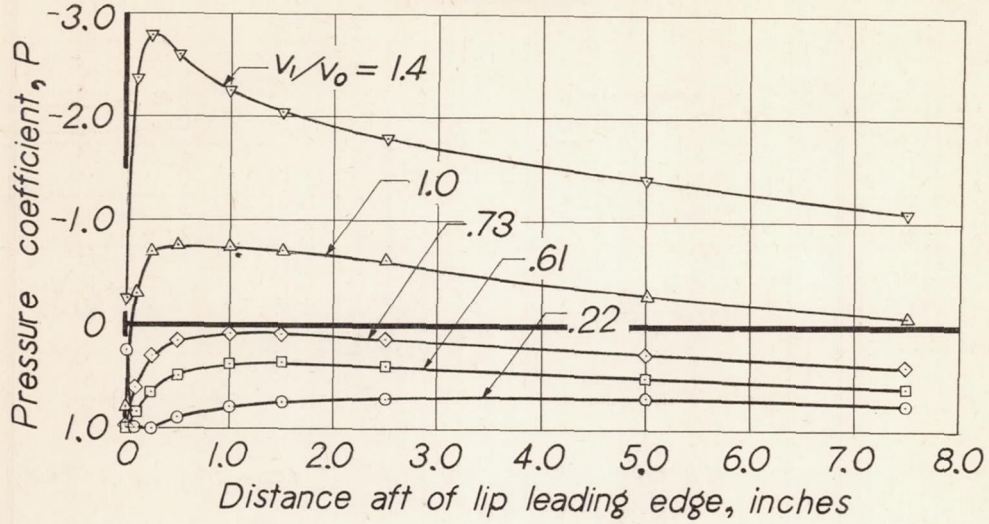

(a) Lip inner surface

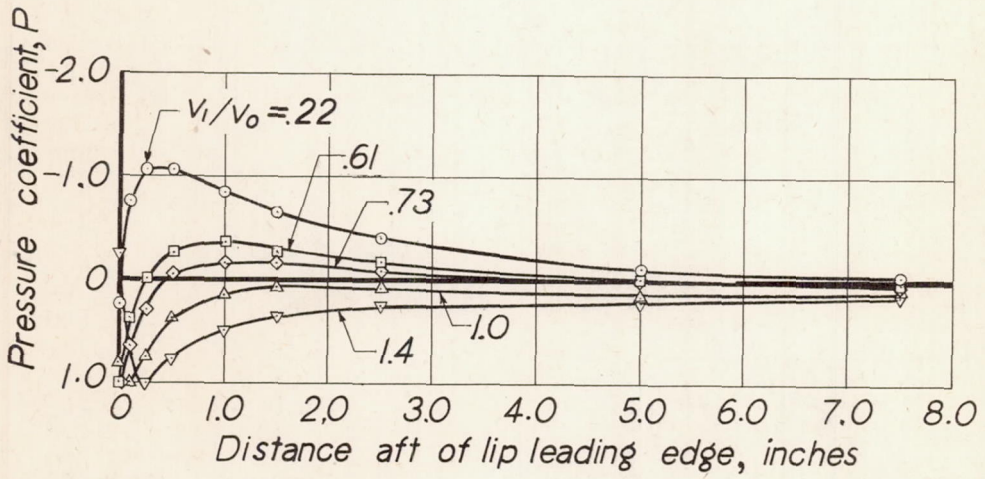

(b) Lip outer surface.

NACA

Figure 23.- The pressure distribution over the center line of the lip at various inlet-velocity ratios for the 7° standard curved-diverging ramp, $\alpha = -2°$.

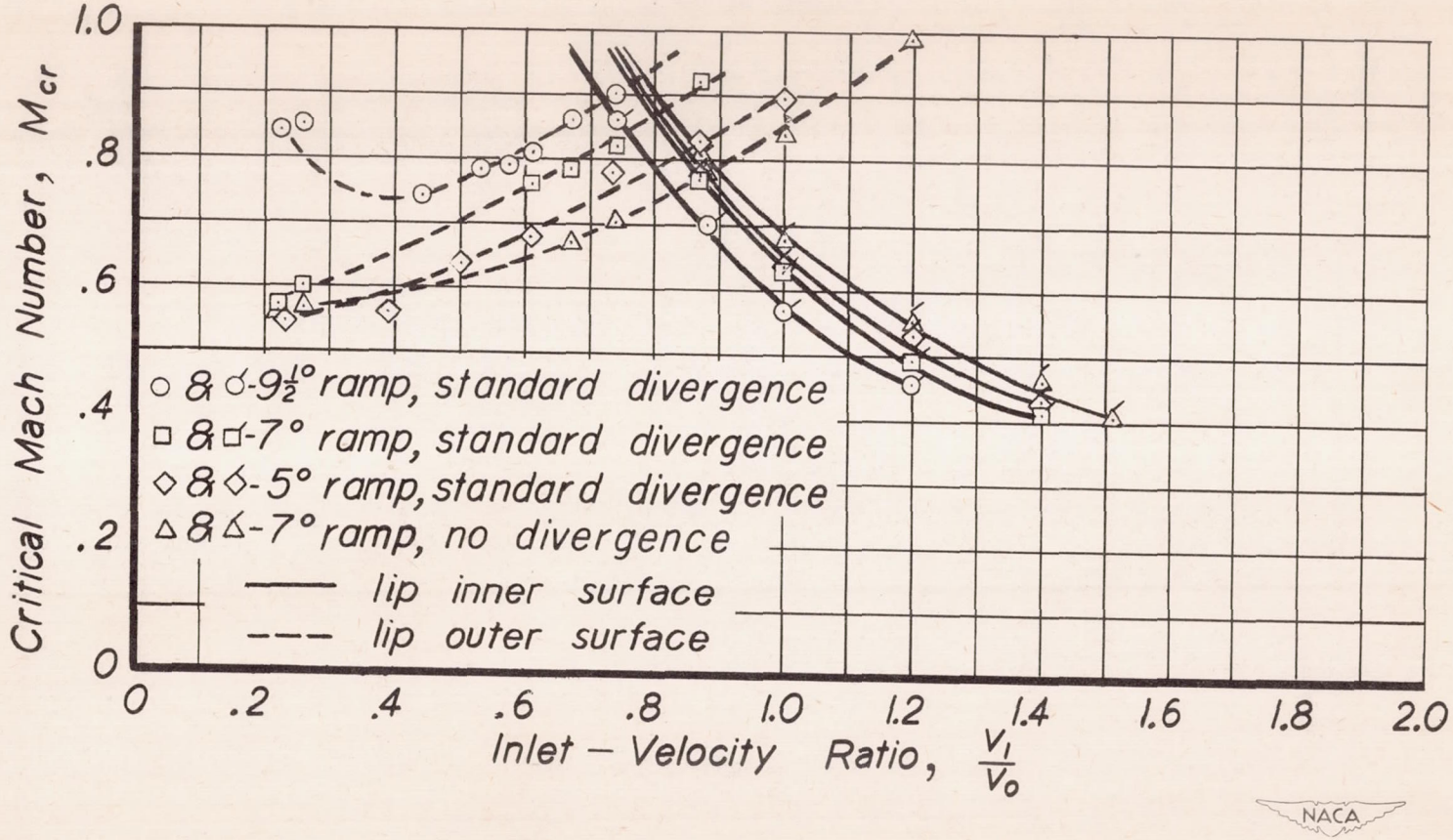

Figure 24.– Variation of critical Mach number along the center line of the lip with inlet velocity, α =-2°.

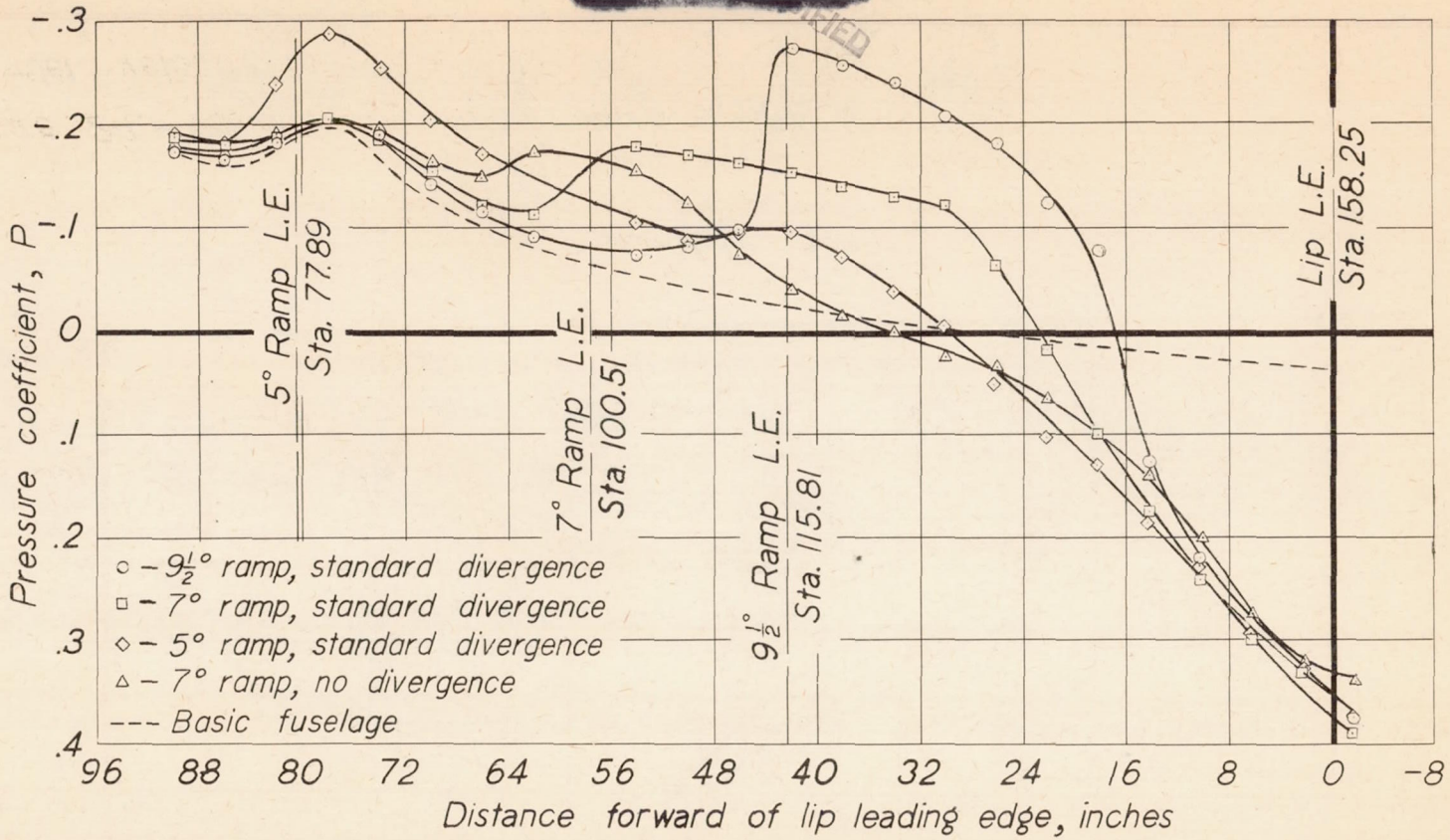

Figure 25.- The pressure distribution along the center line of various ramps at inlet–velocity ratio of 0.74.

UNCLASSIFIED